2. MODELING OF PARALLEL THREE-PHASE CURRENT-BIDIRECTIONAL CONVERTERS

This chapter develops the models of the parallel three-phase current-bidirectional switch based PWM converters, which include three-phase AC/DC boost rectifiers and DC/AC voltage source inverters.

2.1 TOPOLOGIES AND PARALLEL ARCHITECTURES

A three-phase boost rectifier and a three-phase voltage source inverter are shown in Figures 2.1 and 2.2, respectively. To simplify the discussion, the load for both converters is resistive.

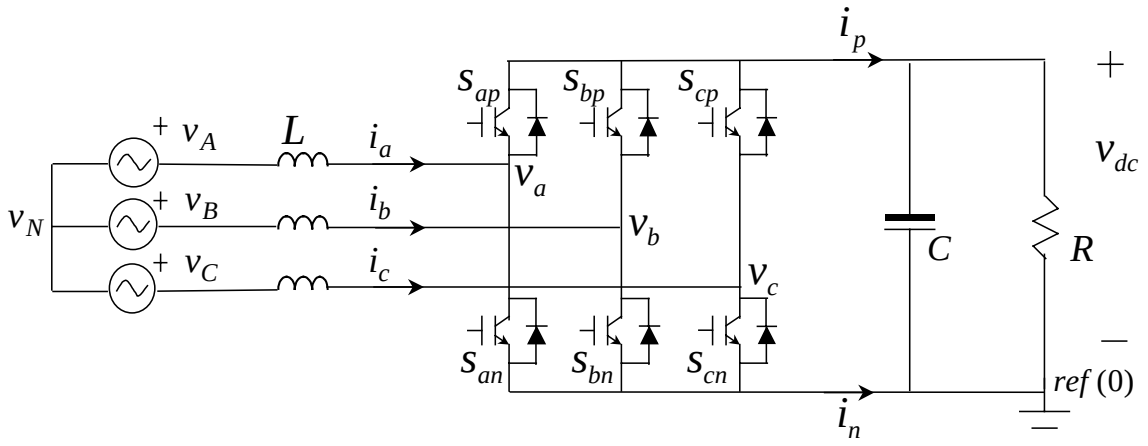

Figure 2.1 Three-phase boost rectifier.

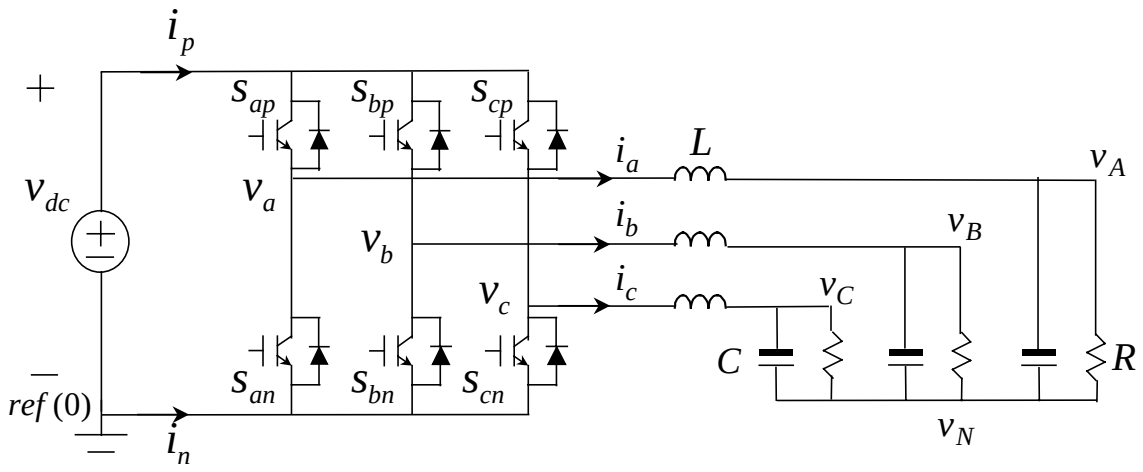

Figure 2.2 Three-phase voltage source inverter.

Both boost rectifier and voltage source inverter are usually classified as current-bidirectional converters because they share the same switching cells that are current bidirectional. The switching cells either inherently have anti-parallel diodes, for example, IGBTs and MOSFETs, or have external anti-parallel diodes, for example, GTOs with anti-parallel diodes. The symbolic representation and its voltage and current operational states are shown in Figure 2.3. The symbol normally stands for an IGBT device.

(a) Symbolic representation. (b) Voltage and current operational states.

Figure 2.3 Current-bidirectional switching cell.

In this chapter, the average large-signal models and the small-signal models of the parallel three-phase current-bidirectional converters are developed. The switching network averaging is performed on a phase-leg basis. Conventionally, the averaging for a three-phase current-bidirectional converter is based on phase-to-phase (or line-to-line) averaging, which intentionally neglects common-mode components [52], [53]. The common-mode components are generally of no interest in the control design for a single three-phase converter. However, they are critical in the analysis and design of parallel converters. The phase-leg averaging adopts a reference point in the system, then derives

the average values of all other points referring to the reference point. As a result, it allows the model to preserve the common-mode components. After the phase-leg averaging, the average model of a three-phase current-bidirectional converter can be easily obtained by connecting three averaged phase legs.

For simplicity, a star connection is used for the AC side of the circuits in Figures 2.1 and 2.2. An actual delta connection can always be converted to the star connection based on Norton or Thevenin theorems. Besides, the reference point of the converter is chosen at the negative rail of the DC bus, as shown in Figures 2.1 and 2.2. The choice of the reference point does not have any particular purpose except for a simple representation for modeling. If another point is chosen, all voltage potentials will be shifted by a constant value.

Figures 2.4 and 2.5 show the parallel three-phase boost rectifiers and the parallel three-phase voltage source inverters, respectively. Assuming the parallel converter systems double the power rating, then the output capacitance becomes $2C$, and the output resistance becomes $R/2$, where C and R are the parameters of a single converter in Figures 2.1 and 2.2, respectively.

One distinguishing feature of the directly parallel three-phase converters is a circulating current. Figures 2.4 and 2.5 show a possible circulating current path in the two parallel systems.

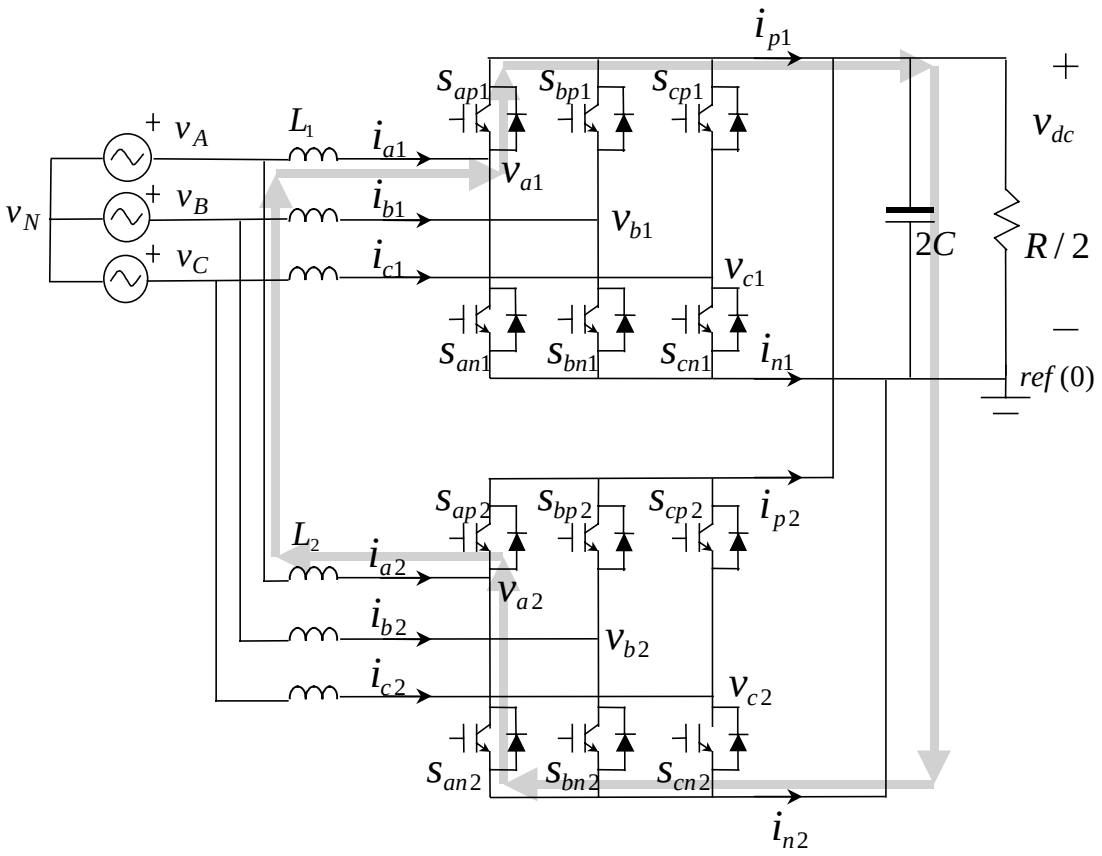

Figure 2.4 Circulating current in parallel three-phase boost rectifiers.

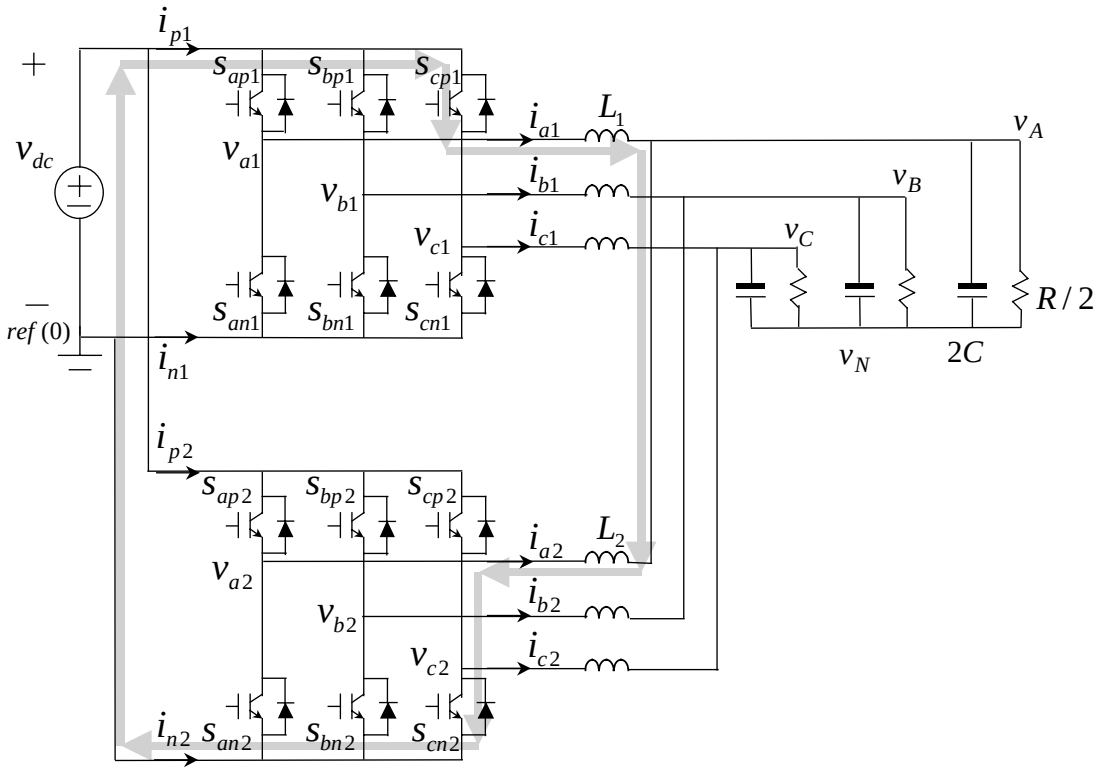

Figure 2.5 Circulating current in parallel three-phase voltage-source inverters.

It can be seen in Figures 2.4 and 2.5 that more than one circulating current path exists. Instead of looking at all individual circulating currents, a zero-sequence current is normally defined to represent the overall circulating current. The zero-sequence current is defined as the sum of all phases' currents in one converter, i.e. referring to Figures 2.1 and 2.2.

$$i_z = i_a + i_b + i_c = i_p + i_n . \tag{2.1}$$

In a single converter operation, the zero-sequence current is always zero because physically there is no such current path. In parallel converters, however, the current is no longer always zero because of the circulating current paths. Therefore, appropriate controls have to be applied in order to suppress the zero-sequence current because of its adverse effects, such as additional conduction losses, overrun devices rating, distorted waveforms, etc. Before proposing controls, the models of the parallel converter systems will be developed in the next sections.

2.2 AVERAGE MODELS

2.2.1 Phase-Leg Averaging

The switching cell in Figure 2.3(a) can be described by a generic switch s, as shown in Figure 2.6.

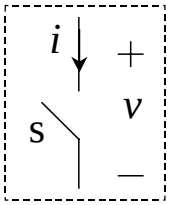

Figure 2.6 Generic switch s.

When s is open, that is, neither the switch itself nor the anti-parallel diode conducts, referring to Figure 2.3(a), then the current *i* is zero. When s is closed, that is, either the switch itself or the anti-parallel diode conducts, the voltage *v* is then zero. Therefore, a switching function *s* can be defined as follows:

$$s = \begin{cases} 0,\ i = 0, \text{ if switch s is open,} \\ 1,\ v = 0, \text{ if switch s is closed.} \end{cases} \tag{2.2}$$

In the current-bidirectional switch based converters, a generic switching unit, called a phase leg, can be identified, as shown in Figure 2.7. The phase leg is composed of two switching cells, and has a voltage source (or a capacitor) on one side and a current source (or an inductor) on the other. These features make the phase leg a generic switching unit.

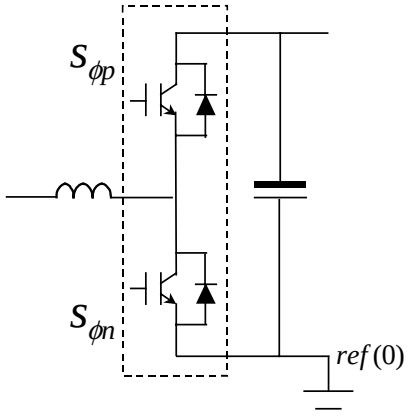

Figure 2.7 Generic phase leg in current-bidirectional converters.

There are switching constraints for the two switching cells of the phase leg. The constraints include that voltage sources or capacitors cannot be short-circuited, and current sources or inductors cannot be open-circuited. The constraints result in a requirement that the two switching cells of the phase leg are complementary. That is, to prevent the voltage source (or the capacitor) from being short-circuited, only one of the two switching cells, $s_{\phi p}$ and $s_{\phi n}$, can be closed at any time. Meanwhile, to prevent the inductor from being open-circuited, one of the two switching cells has to be closed at any time. Based on the switching function defined in (2.2), this complementary relationship can be described as:

$$s_{\phi p} + s_{\phi n} = 1. \tag{2.3}$$

As a result, the phase leg can be represented by a single-pole, double-throw switch, as shown in Figure 2.8. The input and output variables of interest are also defined in Figure 2.8. Because the currents of the positive and negative DC rails are not necessarily equal in the parallel converters, i_p and i_n are defined as the current of the positive and negative DC rails, respectively, referring to Figures 2.1 and 2.2.

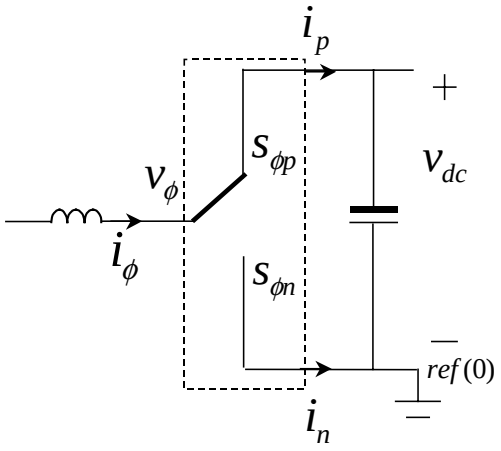

Figure 2.8 Phase leg represented as a single-pole, double-throw switch.

The PWM of the phase leg is shown in Figure 2.9, where T is the switching period and d_ϕ is defined as the duty cycle of the top switch $s_{\phi p}$. The corresponding voltage and current waveforms are also shown in Figure 2.9.

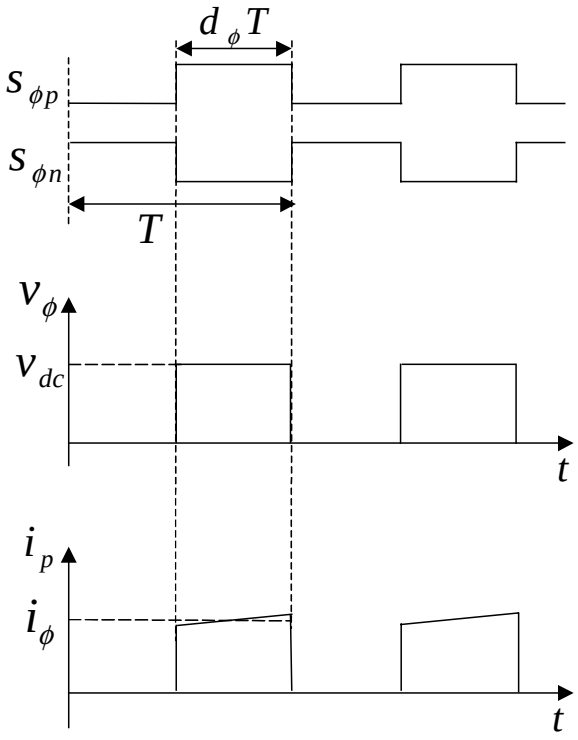

Figure 2.9 Phase leg PWM and corresponding current and voltage waveforms.

Based on the waveforms, one can obtain the voltage and current relationships in average, assuming the current i_ϕ and the voltage v_{dc} are continuous with small ripples:

$$v_\phi = d_\phi \cdot v_{dc}\,, \tag{2.4}$$

$$i_p = d_\phi \cdot i_\phi\,. \tag{2.5}$$

The average model of the phase leg is depicted in Figure 2.10.

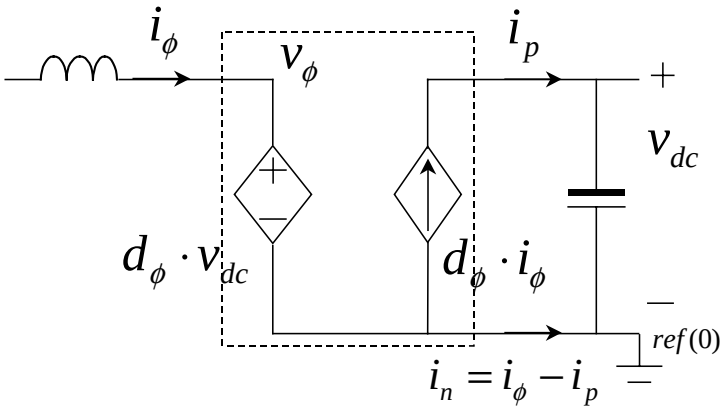

Figure 2.10 Phase leg's average model.

2.2.2 Average Model of Parallel Boost Rectifiers

After averaging the phase leg, the average model of a three-phase boost rectifier can be readily obtained by connecting three averaged phase legs and the rest of the circuit components, as shown in Figure 2.11, where

$$i_p = d_a \cdot i_a + d_b \cdot i_b + d_c \cdot i_c \,, \tag{2.6}$$

$$i_n = i_a + i_b + i_c - i_p = i_z - i_p \,. \tag{2.7}$$

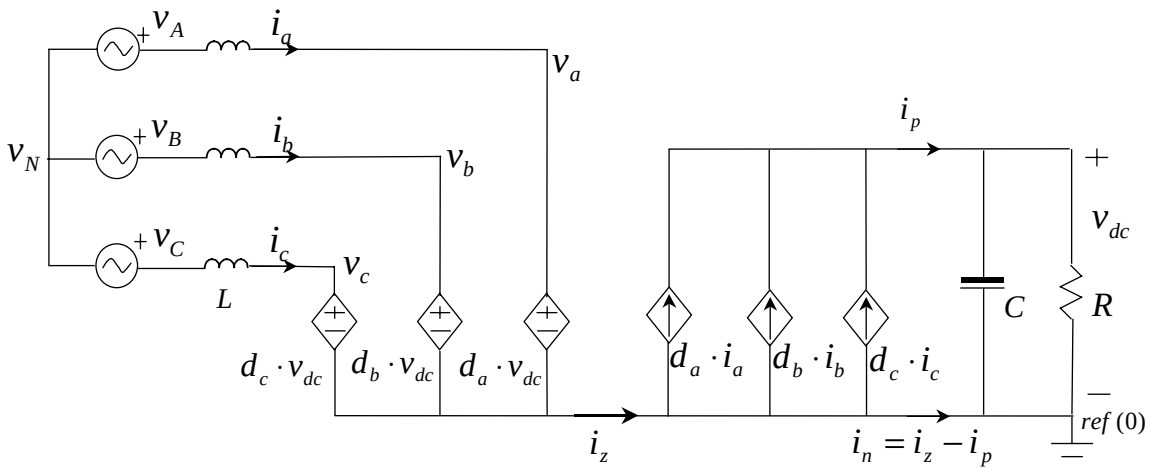

Figure 2.11 Boost rectifier's average model in stationary coordinates.

The state-space equations of the boost rectifier are:

$$\frac{d}{dt}\begin{bmatrix} i_a \\ i_b \\ i_c \end{bmatrix} = \frac{1}{L}\begin{bmatrix} v_{AN} \\ v_{BN} \\ v_{CN} \end{bmatrix} + \frac{1}{L}\begin{bmatrix} v_N \\ v_N \\ v_N \end{bmatrix} - \frac{1}{L}\begin{bmatrix} d_a \\ d_b \\ d_c \end{bmatrix} \cdot v_{dc} \,, \tag{2.8}$$

$$\frac{dv_{dc}}{dt} = \frac{1}{C}\begin{bmatrix} d_a & d_b & d_c \end{bmatrix} \cdot \begin{bmatrix} i_a \\ i_b \\ i_c \end{bmatrix} - \frac{v_{dc}}{RC} \,. \tag{2.9}$$

It can be seen from Figure 2.11 that, in a single converter, the zero-sequence current is always zero because physically there is no such current path. With the parallel operation, however, a circulating current path is formed, as shown in Figure 2.12, and noting that:

$$i_z = i_{z1} = -i_{z2} \,. \tag{2.10}$$

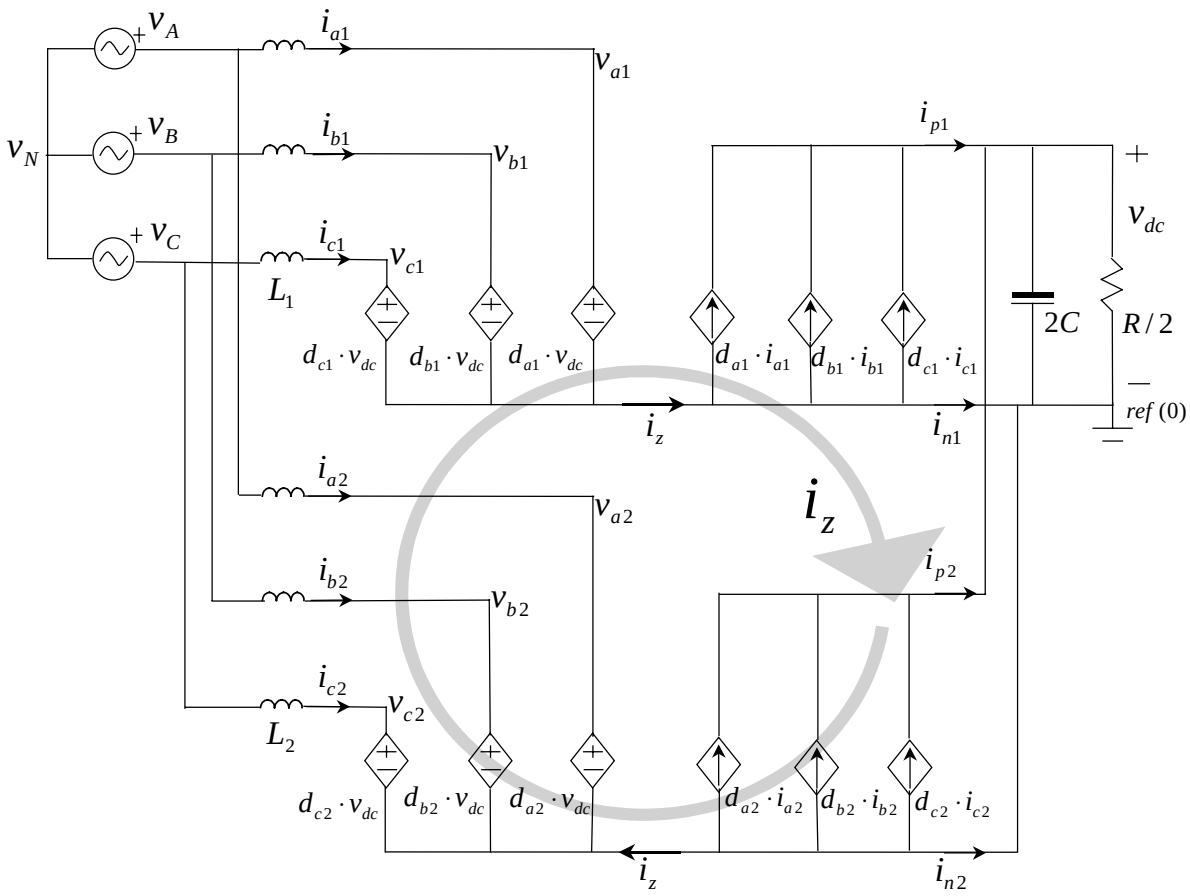

Figure 2.12 Parallel boost rectifiers' average model in stationary coordinates.

The state-space equations of the parallel boost rectifiers are:

$$\frac{d}{dt}\begin{bmatrix} i_{a1} \\ i_{b1} \\ i_{c1} \end{bmatrix} = \frac{1}{L_1}\begin{bmatrix} v_{AN} \\ v_{BN} \\ v_{CN} \end{bmatrix} + \frac{1}{L_1}\begin{bmatrix} v_N \\ v_N \\ v_N \end{bmatrix} - \frac{1}{L_1}\begin{bmatrix} d_{a1} \\ d_{b1} \\ d_{c1} \end{bmatrix} \cdot v_{dc}\,, \tag{2.11}$$

$$\frac{d}{dt}\begin{bmatrix} i_{a2} \\ i_{b2} \\ i_{c2} \end{bmatrix} = \frac{1}{L_2}\begin{bmatrix} v_{AN} \\ v_{BN} \\ v_{CN} \end{bmatrix} + \frac{1}{L_2}\begin{bmatrix} v_N \\ v_N \\ v_N \end{bmatrix} - \frac{1}{L_2}\begin{bmatrix} d_{a2} \\ d_{b2} \\ d_{c2} \end{bmatrix} \cdot v_{dc}\,, \tag{2.12}$$

$$\frac{dv_{dc}}{dt} = \frac{1}{2C}\left(\begin{bmatrix} d_{a1} & d_{b1} & d_{c1} \end{bmatrix} \cdot \begin{bmatrix} i_{a1} \\ i_{b1} \\ i_{c1} \end{bmatrix} + \begin{bmatrix} d_{a2} & d_{b2} & d_{c2} \end{bmatrix} \cdot \begin{bmatrix} i_{a2} \\ i_{b2} \\ i_{c2} \end{bmatrix}\right) - \frac{v_{dc}}{RC}\,. \tag{2.13}$$

In steady state, the output DC voltage v_{dc} is controlled as a constant value. The phase currents i_{a1}, i_{b1}, i_{c1}, i_{a2}, i_{b2} and i_{c2} are controlled to be sinusoidal and in phase with the corresponding input phase voltages v_{AN}, v_{BN} and v_{CN}, which are normally given, for example,

$$\begin{bmatrix} v_{AN} \\ v_{BN} \\ v_{CN} \end{bmatrix} = \begin{bmatrix} V_m \cos(\omega t) \\ V_m \cos(\omega t - 2\pi/3) \\ V_m \cos(\omega t + 2\pi/3) \end{bmatrix}. \tag{2.14}$$

In order to obtain a DC steady-state operating point so as to linearize the system to design controllers, the model in the stationary coordinates is usually transformed into rotating coordinates.

The transformation matrix is chosen as follows:

$$T = \sqrt{\frac{2}{3}} \begin{bmatrix} \cos\omega t & \cos(\omega t - \frac{2\pi}{3}) & \cos(\omega t + \frac{2\pi}{3}) \\ -\sin\omega t & -\sin(\omega t - \frac{2\pi}{3}) & -\sin(\omega t + \frac{2\pi}{3}) \\ \frac{1}{\sqrt{2}} & \frac{1}{\sqrt{2}} & \frac{1}{\sqrt{2}} \end{bmatrix}, \tag{2.15}$$

where ω is chosen as the same frequency as the AC line frequency in (2.14). T is an orthogonal matrix.

The variables in the stationary coordinates X_{abc} can be transformed into the rotating coordinates X_{dqz} using

$$X_{dqz} = T \cdot X_{abc}. \tag{2.16}$$

Applying (2.16) to (2.8)-(2.9), one can obtain the average model of a single boost rectifier in the rotating coordinates:

$$\frac{d}{dt}\begin{bmatrix} i_d \\ i_q \\ i_z \end{bmatrix} = \frac{1}{L}\begin{bmatrix} v_d \\ v_q \\ v_z \end{bmatrix} + \frac{1}{L}\begin{bmatrix} 0 \\ 0 \\ 3v_N \end{bmatrix} - \begin{bmatrix} 0 & -\omega & 0 \\ \omega & 0 & 0 \\ 0 & 0 & 0 \end{bmatrix} \cdot \begin{bmatrix} i_d \\ i_q \\ i_z \end{bmatrix} - \frac{1}{L}\begin{bmatrix} d_d \\ d_q \\ d_z \end{bmatrix} \cdot v_{dc}, \tag{2.17}$$

$$\frac{dv_{dc}}{dt} = \frac{1}{C}\begin{bmatrix} d_d & d_q & d_z/3 \end{bmatrix} \cdot \begin{bmatrix} i_d \\ i_q \\ i_z \end{bmatrix} - \frac{v_{dc}}{RC}. \tag{2.18}$$

where:

$$\begin{bmatrix} i_d \\ i_q \\ i_z/\sqrt{3} \end{bmatrix} = T \cdot \begin{bmatrix} i_a \\ i_b \\ i_c \end{bmatrix}, \begin{bmatrix} v_d \\ v_q \\ v_z/\sqrt{3} \end{bmatrix} = T \cdot \begin{bmatrix} v_{AN} \\ v_{BN} \\ v_{CN} \end{bmatrix}, \begin{bmatrix} d_d \\ d_q \\ d_z/\sqrt{3} \end{bmatrix} = T \cdot \begin{bmatrix} d_a \\ d_b \\ d_c \end{bmatrix}. \tag{2.19}$$

Be noted that i_z is defined in (2.1), and v_z , d_z are defined as:

$$v_z = v_{AN} + v_{BN} + v_{CN}\,, \qquad d_z = d_a + d_b + d_c\,. \tag{2.20}$$

Since $i_z \equiv 0$ in the single converter operation, the z-channel equation is normally dropped from the model. Therefore, the average model of the single boost rectifier becomes

$$\frac{d}{dt}\begin{bmatrix} i_d \\ i_q \end{bmatrix} = \frac{1}{L}\begin{bmatrix} v_d \\ v_q \end{bmatrix} - \begin{bmatrix} 0 & -\omega \\ \omega & 0 \end{bmatrix} \cdot \begin{bmatrix} i_d \\ i_q \end{bmatrix} - \frac{1}{L}\begin{bmatrix} d_d \\ d_q \end{bmatrix} \cdot v_{dc}\,, \tag{2.21}$$

$$\frac{dv_{dc}}{dt} = \frac{1}{C}\begin{bmatrix} d_d & d_q \end{bmatrix} \cdot \begin{bmatrix} i_d \\ i_q \end{bmatrix} - \frac{v_{dc}}{RC}\,. \tag{2.22}$$

Figure 2.13 shows the equivalent circuit of the model. While the model differs from the one based on phase-to-phase averaging by only some coefficients, the topologies are the same [53].

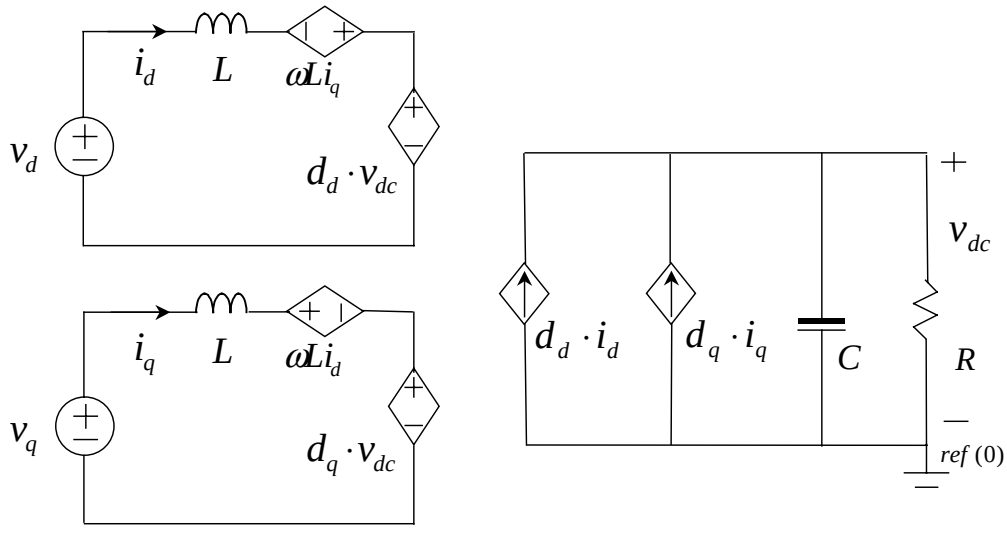

Figure 2.13 Boost rectifier's average model in rotating coordinates.

Applying (2.16) to (2.11)-(2.13), one can obtain the average model of the parallel boost rectifiers in the rotating coordinates:

$$\frac{d}{dt}\begin{bmatrix} i_{d1} \\ i_{q1} \\ i_{z1} \end{bmatrix} = \frac{1}{L_1}\begin{bmatrix} v_d \\ v_q \\ v_z \end{bmatrix} + \frac{1}{L_1}\begin{bmatrix} 0 \\ 0 \\ 3v_N \end{bmatrix} - \begin{bmatrix} 0 & -\omega & 0 \\ \omega & 0 & 0 \\ 0 & 0 & 0 \end{bmatrix} \cdot \begin{bmatrix} i_{d1} \\ i_{q1} \\ i_{z1} \end{bmatrix} - \frac{1}{L_1}\begin{bmatrix} d_{d1} \\ d_{q1} \\ d_{z1} \end{bmatrix} \cdot v_{dc} \tag{2.23}$$

$$\frac{d}{dt}\begin{bmatrix} i_{d2} \\ i_{q2} \\ i_{z2} \end{bmatrix} = \frac{1}{L_2}\begin{bmatrix} v_d \\ v_q \\ v_z \end{bmatrix} + \frac{1}{L_2}\begin{bmatrix} 0 \\ 0 \\ 3v_N \end{bmatrix} - \begin{bmatrix} 0 & -\omega & 0 \\ \omega & 0 & 0 \\ 0 & 0 & 0 \end{bmatrix} \cdot \begin{bmatrix} i_{d2} \\ i_{q2} \\ i_{z2} \end{bmatrix} - \frac{1}{L_2}\begin{bmatrix} d_{d2} \\ d_{q2} \\ d_{z2} \end{bmatrix} \cdot v_{dc}, \tag{2.24}$$

$$\frac{dv_{dc}}{dt} = \frac{1}{2C}\left(\begin{bmatrix} d_{d1} & d_{q1} & d_{z1}/3 \end{bmatrix} \cdot \begin{bmatrix} i_{d1} \\ i_{q1} \\ i_{z1} \end{bmatrix} + \begin{bmatrix} d_{d2} & d_{q2} & d_{z2}/3 \end{bmatrix} \cdot \begin{bmatrix} i_{d2} \\ i_{q2} \\ i_{z2} \end{bmatrix}\right) - \frac{v_{dc}}{RC}. \tag{2.25}$$

Because of the definition in (2.10), the above equations can be simplified as follows:

$$\frac{d}{dt}\begin{bmatrix} i_{d1} \\ i_{q1} \end{bmatrix} = \frac{1}{L_1} \cdot \begin{bmatrix} v_d \\ v_q \end{bmatrix} - \begin{bmatrix} 0 & -\omega \\ \omega & 0 \end{bmatrix} \cdot \begin{bmatrix} i_{d1} \\ i_{q1} \end{bmatrix} - \frac{1}{L_1} \cdot \begin{bmatrix} d_{d1} \\ d_{q1} \end{bmatrix} \cdot v_{dc}, \tag{2.26}$$

$$\frac{d}{dt}\begin{bmatrix} i_{d2} \\ i_{q2} \end{bmatrix} = \frac{1}{L_2} \cdot \begin{bmatrix} v_d \\ v_q \end{bmatrix} - \begin{bmatrix} 0 & -\omega \\ \omega & 0 \end{bmatrix} \cdot \begin{bmatrix} i_{d2} \\ i_{q2} \end{bmatrix} - \frac{1}{L_2} \cdot \begin{bmatrix} d_{d2} \\ d_{q2} \end{bmatrix} \cdot v_{dc}, \tag{2.27}$$

$$\frac{di_z}{dt} = -\frac{\Delta d_z \cdot v_{dc}}{L_1 + L_2}, \tag{2.28}$$

$$\frac{dv_{dc}}{dt} = \frac{1}{2C}\left(\begin{bmatrix} d_{d1} & d_{q1} \end{bmatrix} \cdot \begin{bmatrix} i_{d1} \\ i_{q1} \end{bmatrix} + \begin{bmatrix} d_{d2} & d_{q2} \end{bmatrix} \cdot \begin{bmatrix} i_{d2} \\ i_{q2} \end{bmatrix} + \frac{\Delta d_z \cdot i_z}{3}\right) - \frac{v_{dc}}{RC}, \tag{2.29}$$

where

$$\Delta d_z = d_{z1} - d_{z2}. \tag{2.30}$$

The equivalent circuit of the model is shown in Figure 2.14. It can be seen that a zero-sequence current is now present in the z channel. Whereas it was previously dropped in the single converter model, it now plays a significant role in the parallel model.

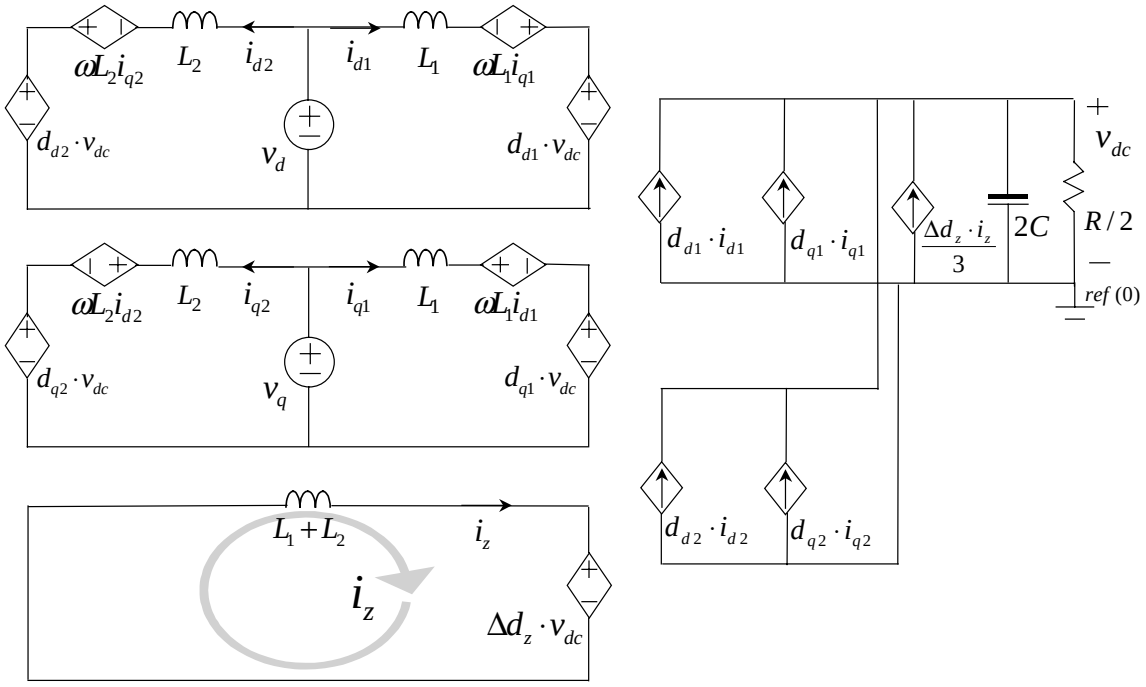

Figure 2.14 Parallel boost rectifiers' average model in rotating coordinates.

2.2.3 Average Model of Parallel Voltage Source Inverters

The average model of a three-phase voltage source inverter can be obtained by connecting three averaged phase legs and the rest of the circuit components, as shown in Figure 2.15.

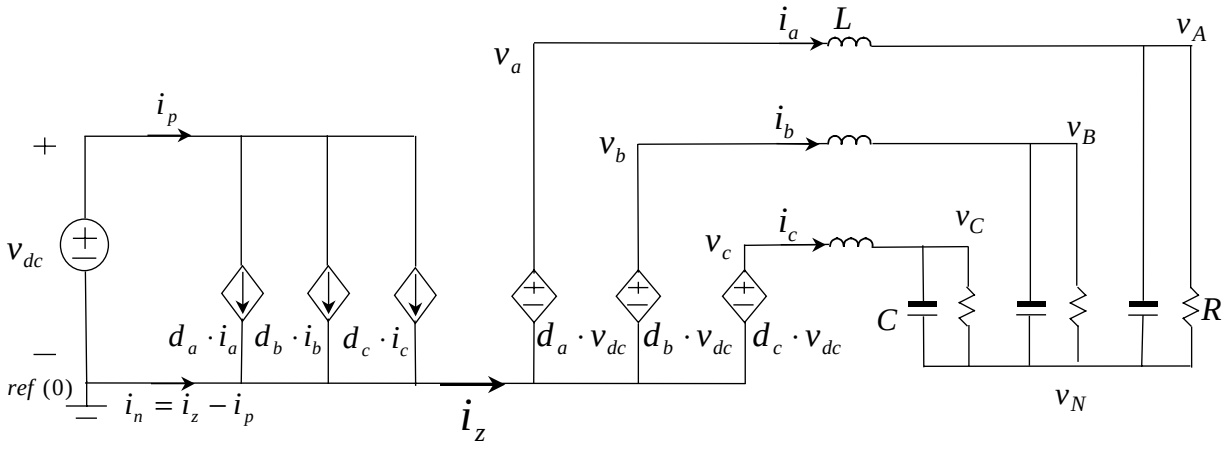

Figure 2.15 Voltage-source inverter's average model in stationary coordinates.

The state-space equations of the voltage source inverter are:

$$\frac{d}{dt}\begin{bmatrix} i_a \\ i_b \\ i_c \end{bmatrix} = \frac{1}{L}\begin{bmatrix} d_a \\ d_b \\ d_c \end{bmatrix} \cdot v_{dc} - \frac{1}{L}\begin{bmatrix} v_{AN} \\ v_{BN} \\ v_{CN} \end{bmatrix} - \frac{1}{L}\begin{bmatrix} v_N \\ v_N \\ v_N \end{bmatrix}, \tag{2.31}$$

$$\frac{d}{dt}\begin{bmatrix} v_{AN} \\ v_{BN} \\ v_{CN} \end{bmatrix} = \frac{1}{C}\begin{bmatrix} i_a \\ i_b \\ i_c \end{bmatrix} - \frac{1}{RC}\begin{bmatrix} v_{AN} \\ v_{BN} \\ v_{CN} \end{bmatrix}. \tag{2.32}$$

As can be seen from Figure 2.15, the zero-sequence current is always zero because physically there is no such current path. In parallel operation, however, a circulating current path is formed, as shown in Figure 2.16.

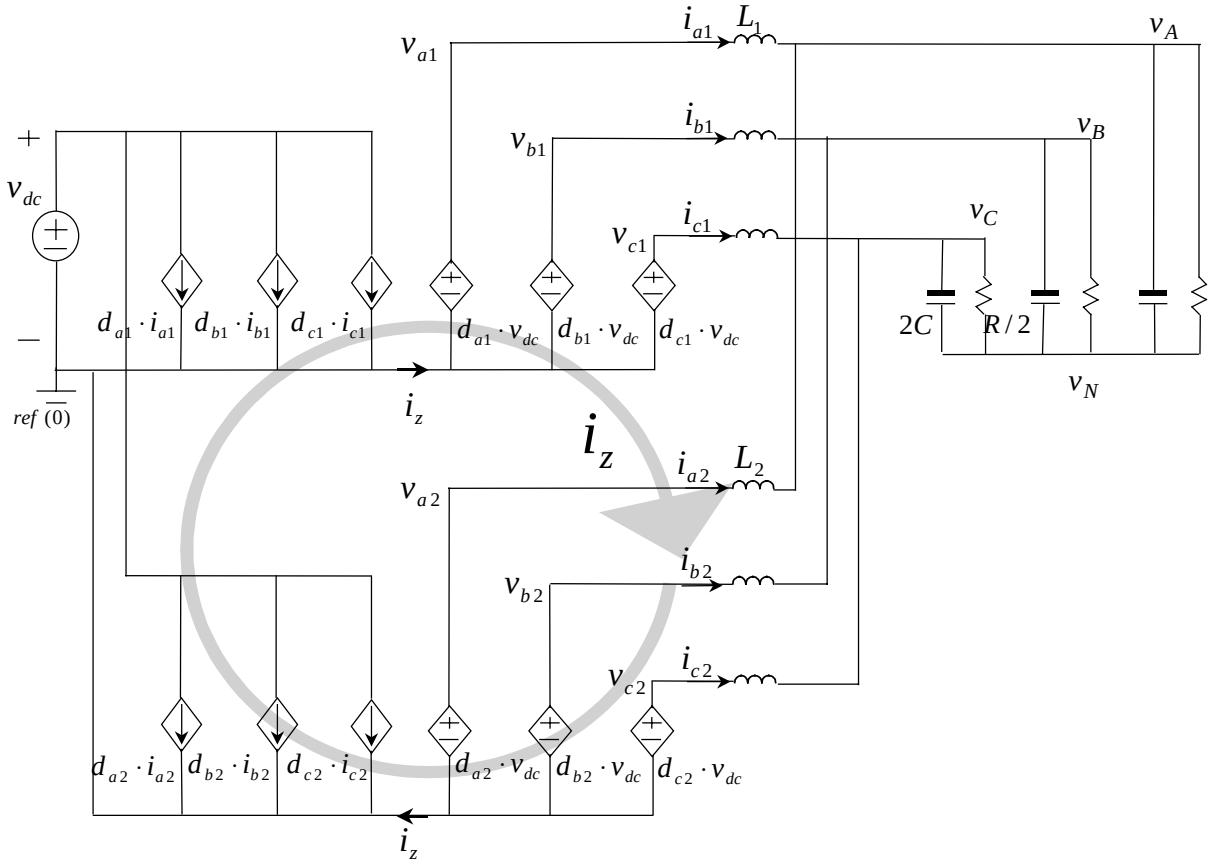

Figure 2.16 Parallel voltage-source inverters' average model in stationary coordinates.

The state-space equations of the parallel voltage source inverters are:

$$\frac{d}{dt}\begin{bmatrix} i_{a1} \\ i_{b1} \\ i_{c1} \end{bmatrix} = \frac{1}{L_1}\begin{bmatrix} d_{a1} \\ d_{b1} \\ d_{c1} \end{bmatrix} \cdot v_{dc} - \frac{1}{L_1}\begin{bmatrix} v_{AN} \\ v_{BN} \\ v_{CN} \end{bmatrix} - \frac{1}{L_1}\begin{bmatrix} v_N \\ v_N \\ v_N \end{bmatrix}, \tag{2.33}$$

$$\frac{d}{dt}\begin{bmatrix} i_{a2} \\ i_{b2} \\ i_{c2} \end{bmatrix} = \frac{1}{L_2}\begin{bmatrix} d_{a2} \\ d_{b2} \\ d_{c2} \end{bmatrix} \cdot v_{dc} - \frac{1}{L_2}\begin{bmatrix} v_{AN} \\ v_{BN} \\ v_{CN} \end{bmatrix} - \frac{1}{L_2}\begin{bmatrix} v_N \\ v_N \\ v_N \end{bmatrix}, \tag{2.34}$$

$$\frac{d}{dt}\begin{bmatrix} v_{AN} \\ v_{BN} \\ v_{CN} \end{bmatrix} = \frac{1}{2C}\begin{bmatrix} i_{a1} \\ i_{b1} \\ i_{c1} \end{bmatrix} + \frac{1}{2C}\begin{bmatrix} i_{a2} \\ i_{b2} \\ i_{c2} \end{bmatrix} - \frac{1}{RC}\begin{bmatrix} v_{AN} \\ v_{BN} \\ v_{CN} \end{bmatrix}. \tag{2.35}$$

In steady state, the output AC voltages v_{AN}, v_{BN} and v_{CN} are regulated as balanced sinusoidal voltage sources. An example is shown in (2.14).

Applying (2.16) to (2.31)-(2.32), one can obtain the average model of the voltage source inverter in the rotating coordinates:

$$\frac{d}{dt}\begin{bmatrix} i_d \\ i_q \\ i_z \end{bmatrix} = \frac{1}{L}\begin{bmatrix} d_d \\ d_q \\ d_z \end{bmatrix} \cdot v_{dc} - \frac{1}{L}\begin{bmatrix} v_d \\ v_q \\ v_z \end{bmatrix} - \frac{1}{L}\begin{bmatrix} 0 \\ 0 \\ 3v_N \end{bmatrix} - \begin{bmatrix} 0 & -\omega & 0 \\ \omega & 0 & 0 \\ 0 & 0 & 0 \end{bmatrix} \cdot \begin{bmatrix} i_d \\ i_q \\ i_z \end{bmatrix}, \tag{2.36}$$

$$\frac{d}{dt}\begin{bmatrix} v_d \\ v_q \\ v_z \end{bmatrix} = \frac{1}{C}\begin{bmatrix} i_d \\ i_q \\ i_z \end{bmatrix} - \frac{1}{RC}\begin{bmatrix} v_d \\ v_q \\ v_z \end{bmatrix} - \begin{bmatrix} 0 & -\omega & 0 \\ \omega & 0 & 0 \\ 0 & 0 & 0 \end{bmatrix} \cdot \begin{bmatrix} v_d \\ v_q \\ v_z \end{bmatrix}. \tag{2.37}$$

Since $i_z \equiv 0$ in the single converter, the z-channel equation is normally dropped from the model. Therefore, the average model of the single voltage source inverter becomes:

$$\frac{d}{dt}\begin{bmatrix} i_d \\ i_q \end{bmatrix} = \frac{1}{L}\begin{bmatrix} d_d \\ d_q \end{bmatrix} \cdot v_{dc} - \frac{1}{L}\begin{bmatrix} v_d \\ v_q \end{bmatrix} - \begin{bmatrix} 0 & -\omega \\ \omega & 0 \end{bmatrix} \cdot \begin{bmatrix} i_d \\ i_q \end{bmatrix}, \tag{2.38}$$

$$\frac{d}{dt}\begin{bmatrix} v_d \\ v_q \end{bmatrix} = \frac{1}{C}\begin{bmatrix} i_d \\ i_q \end{bmatrix} - \frac{1}{RC}\begin{bmatrix} v_d \\ v_q \end{bmatrix} - \begin{bmatrix} 0 & -\omega \\ \omega & 0 \end{bmatrix} \cdot \begin{bmatrix} v_d \\ v_q \end{bmatrix}. \tag{2.39}$$

The equivalent circuit is shown in Figure 2.17. Again, the model is different from the one based on phase-to-phase averaging by only some coefficients, while the topologies are the same [53].

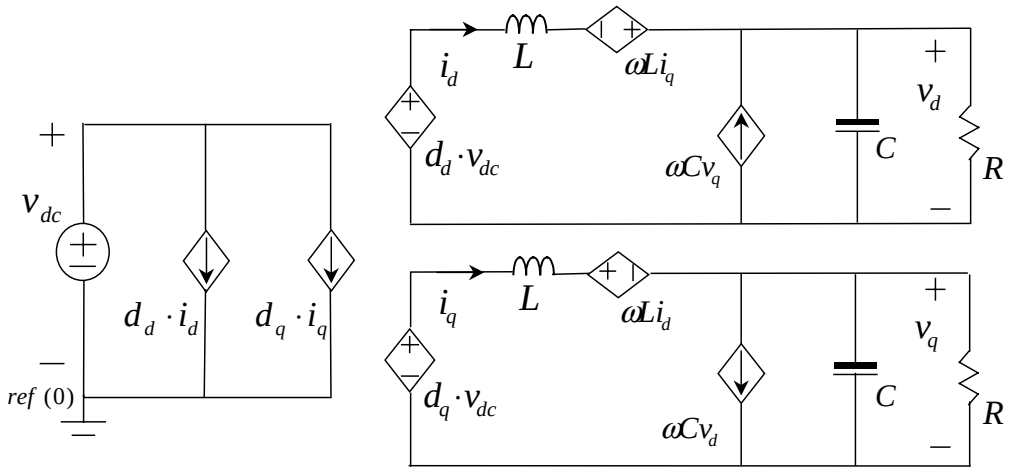

Figure 2.17 Voltage-source inverter's average model in rotating coordinates.

Applying (2.16) to (2.33)-(2.35), one can obtain the average model of the parallel voltage source inverters in the rotating coordinates:

$$\frac{d}{dt}\begin{bmatrix} i_{d1} \\ i_{q1} \\ i_{z1} \end{bmatrix} = \frac{1}{L_1}\begin{bmatrix} d_{d1} \\ d_{q1} \\ d_{z1} \end{bmatrix} \cdot v_{dc} - \frac{1}{L_1}\begin{bmatrix} v_d \\ v_q \\ v_z \end{bmatrix} - \frac{1}{L_1}\begin{bmatrix} 0 \\ 0 \\ 3v_N \end{bmatrix} - \begin{bmatrix} 0 & -\omega & 0 \\ \omega & 0 & 0 \\ 0 & 0 & 0 \end{bmatrix} \cdot \begin{bmatrix} i_{d1} \\ i_{q1} \\ i_{z1} \end{bmatrix}, \tag{2.40}$$

$$\frac{d}{dt}\begin{bmatrix} i_{d2} \\ i_{q2} \\ i_{z2} \end{bmatrix} = \frac{1}{L_2}\begin{bmatrix} d_{d2} \\ d_{q2} \\ d_{z2} \end{bmatrix} \cdot v_{dc} - \frac{1}{L_2}\begin{bmatrix} v_d \\ v_q \\ v_z \end{bmatrix} - \frac{1}{L_2}\begin{bmatrix} 0 \\ 0 \\ 3v_N \end{bmatrix} - \begin{bmatrix} 0 & -\omega & 0 \\ \omega & 0 & 0 \\ 0 & 0 & 0 \end{bmatrix} \cdot \begin{bmatrix} i_{d2} \\ i_{q2} \\ i_{z2} \end{bmatrix}, \tag{2.41}$$

$$\frac{d}{dt}\begin{bmatrix} v_d \\ v_q \\ v_z \end{bmatrix} = \frac{1}{2C}\begin{bmatrix} i_{d1} \\ i_{q1} \\ i_{z1} \end{bmatrix} + \frac{1}{2C}\begin{bmatrix} i_{d2} \\ i_{q2} \\ i_{z2} \end{bmatrix} - \frac{1}{RC}\begin{bmatrix} v_d \\ v_q \\ v_z \end{bmatrix} - \begin{bmatrix} 0 & -\omega & 0 \\ \omega & 0 & 0 \\ 0 & 0 & 0 \end{bmatrix} \cdot \begin{bmatrix} v_d \\ v_q \\ v_z \end{bmatrix}. \tag{2.42}$$

Again, the model can be simplified based on (2.10) and (2.30):

$$\frac{d}{dt}\begin{bmatrix} i_{d1} \\ i_{q1} \end{bmatrix} = \frac{1}{L_1} \cdot \begin{bmatrix} d_{d1} \\ d_{q1} \end{bmatrix} \cdot v_{dc} - \frac{1}{L_1} \cdot \begin{bmatrix} v_d \\ v_q \end{bmatrix} - \begin{bmatrix} 0 & -\omega \\ \omega & 0 \end{bmatrix} \cdot \begin{bmatrix} i_{d1} \\ i_{q1} \end{bmatrix}, \tag{2.43}$$

$$\frac{d}{dt}\begin{bmatrix} i_{d2} \\ i_{q2} \end{bmatrix} = \frac{1}{L_2} \cdot \begin{bmatrix} d_{d2} \\ d_{q2} \end{bmatrix} \cdot v_{dc} - \frac{1}{L_2} \cdot \begin{bmatrix} v_d \\ v_q \end{bmatrix} - \begin{bmatrix} 0 & -\omega \\ \omega & 0 \end{bmatrix} \cdot \begin{bmatrix} i_{d2} \\ i_{q2} \end{bmatrix}, \tag{2.44}$$

$$\frac{di_z}{dt} = \frac{\Delta d_z \cdot v_{dc}}{L_1 + L_2}, \tag{2.45}$$

$$\frac{d}{dt}\begin{bmatrix} v_d \\ v_q \end{bmatrix} = \frac{1}{2C}\cdot\left(\begin{bmatrix} i_{d1} \\ i_{q1} \end{bmatrix} + \begin{bmatrix} i_{d2} \\ i_{q2} \end{bmatrix}\right) - \begin{bmatrix} \frac{1}{RC} & -\omega \\ \omega & \frac{1}{RC} \end{bmatrix}\cdot\begin{bmatrix} v_d \\ v_q \end{bmatrix}. \qquad (2.46)$$

As a result, the equivalent circuit of the model is shown in Figure 2.18.

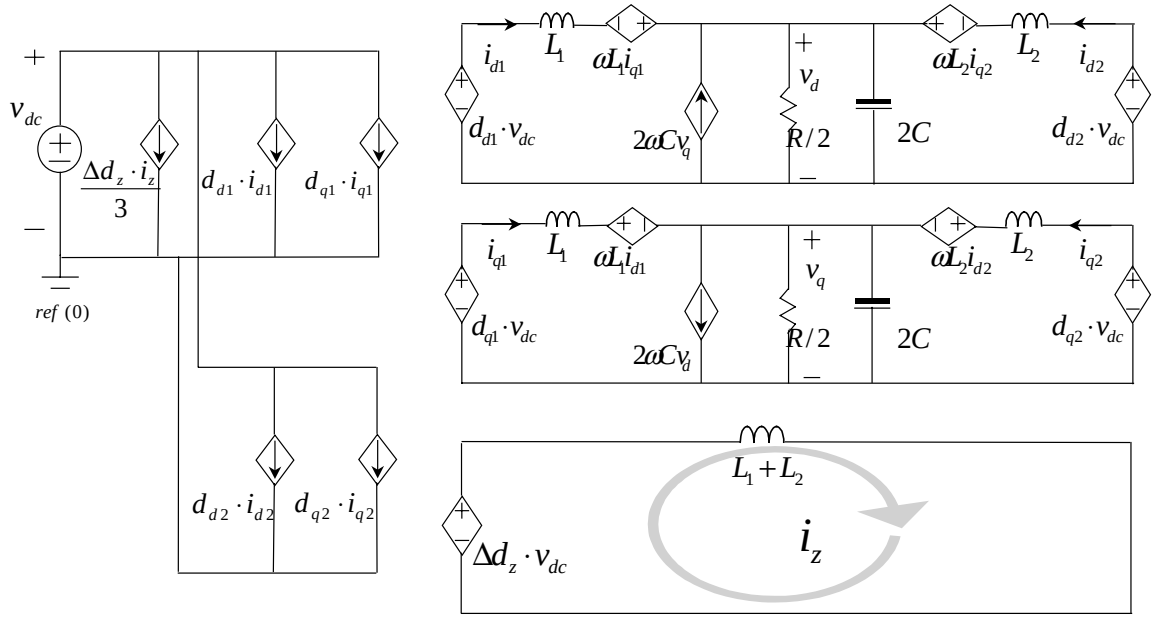

Figure 2.18 Parallel voltage-source inverters' average model in rotating coordinates.

Similar to the situation in the parallel boost rectifiers, a zero-sequence current is present in the z channel, whereas it was previously dropped in the single converter model. It is interesting to note that the z channels of the parallel boost rectifiers and the parallel voltage source inverters are the same except for the current direction.

2.3 SMALL-SIGNAL MODELS

2.3.1 Small-Signal Model of Parallel Boost Rectifiers

To obtain the small-signal model of the parallel three-phase boost rectifiers, a steady-state operating point is obtained first:

$$V_d = \sqrt{\frac{3}{2}}\cdot V_m, \qquad V_q = 0,$$

$$I_{d1} = \frac{V_{dc}}{R \cdot D_{d1}}, \qquad I_{d2} = \frac{V_{dc}}{R \cdot D_{d2}}$$

$$I_{q1} = I_{q2} = 0, \qquad I_z = 0,$$

$$D_{d1} = \frac{V_d}{V_{dc}}, \qquad D_{d2} = \frac{V_d}{V_{dc}}$$

$$D_{q1} = -\frac{\omega L_1 I_{d1}}{V_{dc}}, \quad D_{q2} = -\frac{\omega L_2 I_{d2}}{V_{dc}},$$

$$\Delta D_z = 0, \tag{2.47}$$

where: R, L_1, L_2 and V_m (given as in (2.14)) are given, V_{dc}, I_{q1}, I_{q2} and I_z are controlled to their reference values. I_{d1}, I_{d2}, D_{d1}, D_{d2}, D_{q1}, D_{q2} and ΔD_z are calculated based on the given values and the control objectives.

Assuming that the input voltage sources are ideal, then

$$\tilde{v}_d = \tilde{v}_q = 0. \tag{2.48}$$

The small-signal model of the single boost rectifier can be derived as follows:

$$\frac{d}{dt}\begin{bmatrix} \tilde{v}_{dc} \\ \tilde{i}_d \\ \tilde{i}_q \end{bmatrix} = \begin{bmatrix} \frac{-1}{RC} & \frac{D_d}{C} & \frac{D_q}{C} \\ -\frac{D_d}{L} & 0 & \omega \\ -\frac{D_q}{L} & -\omega & 0 \end{bmatrix} \cdot \begin{bmatrix} \tilde{v}_{dc} \\ \tilde{i}_d \\ \tilde{i}_q \end{bmatrix} + \begin{bmatrix} \frac{I_d}{C} & \frac{I_q}{C} \\ -\frac{V_{dc}}{L} & 0 \\ 0 & -\frac{V_{dc}}{L} \end{bmatrix} \cdot \begin{bmatrix} \tilde{d}_d \\ \tilde{d}_q \end{bmatrix}. \tag{2.49}$$

The small-signal model of the parallel boost rectifiers can be derived as follows:

$$\frac{d}{dt}\begin{bmatrix} \tilde{v}_{dc} \\ \tilde{i}_{d1} \\ \tilde{i}_{q1} \\ \tilde{i}_{d2} \\ \tilde{i}_{q2} \\ \tilde{i}_z \end{bmatrix} = \begin{bmatrix} -\frac{1}{RC} & \frac{D_{d1}}{2C} & \frac{D_{q1}}{2C} & \frac{D_{d2}}{2C} & \frac{D_{q2}}{2C} & 0 \\ -\frac{D_{d1}}{L_1} & 0 & \omega & 0 & 0 & 0 \\ -\frac{D_{q1}}{L_1} & -\omega & 0 & 0 & 0 & 0 \\ -\frac{D_{d2}}{L_2} & 0 & 0 & 0 & \omega & 0 \\ -\frac{D_{q2}}{L_2} & 0 & 0 & -\omega & 0 & 0 \\ 0 & 0 & 0 & 0 & 0 & 0 \end{bmatrix} \cdot \begin{bmatrix} \tilde{v}_{dc} \\ \tilde{i}_{d1} \\ \tilde{i}_{q1} \\ \tilde{i}_{d2} \\ \tilde{i}_{q2} \\ \tilde{i}_z \end{bmatrix} + \begin{bmatrix} \frac{I_{d1}}{2C} & \frac{I_{q1}}{2C} & \frac{I_{d2}}{2C} & \frac{I_{q2}}{2C} & 0 \\ -\frac{V_{dc}}{L_1} & 0 & 0 & 0 & 0 \\ 0 & -\frac{V_{dc}}{L_1} & 0 & 0 & 0 \\ 0 & 0 & -\frac{V_{dc}}{L_2} & 0 & 0 \\ 0 & 0 & 0 & -\frac{V_{dc}}{L_2} & 0 \\ 0 & 0 & 0 & 0 & -\frac{V_{dc}}{L_1+L_2} \end{bmatrix} \cdot \begin{bmatrix} \tilde{d}_{d1} \\ \tilde{d}_{q1} \\ \tilde{d}_{d2} \\ \tilde{d}_{q2} \\ \Delta\tilde{d}_z \end{bmatrix} \tag{2.50}$$

Figure 2.19 shows the equivalent circuit of the small-signal model. Some terms are omitted because $I_z = 0$ and $\Delta D_z = 0$ provided that the zero-sequence current is controlled to be zero, and $I_{q1} = I_{q2} = 0$ provided that the power factor is controlled to be unity. The z channel is totally independent from the d and q channels.

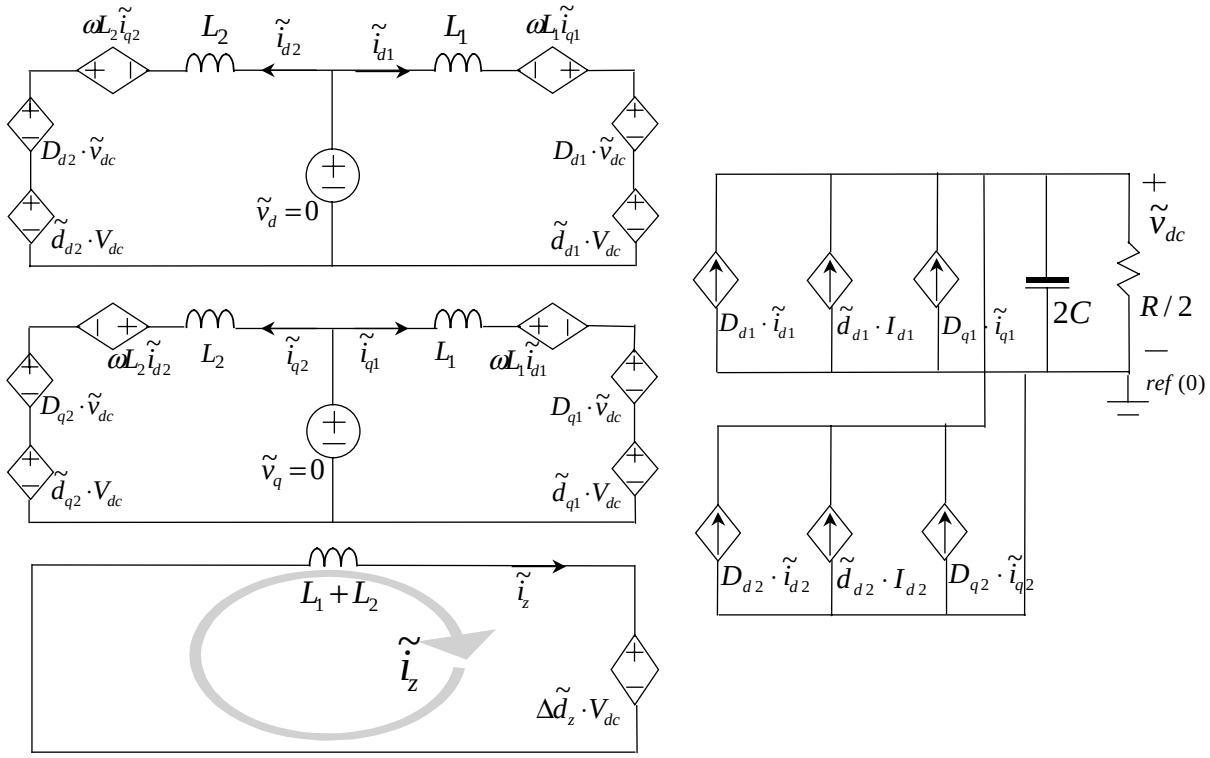

Figure 2.19 Parallel boost rectifiers' small-signal model.

2.3.2 Small-Signal Model of Parallel Voltage Source Inverters

To obtain the small-signal model of the parallel three-phase voltage source inverters, a steady-state operating point is shown below:

$$D_{d1} = \frac{V_d - \omega L_1 I_{q1}}{V_{dc}}, \qquad D_{d2} = \frac{V_d - \omega L_2 I_{q2}}{V_{dc}},$$

$$D_{q1} = \frac{V_q + \omega L_1 I_{d1}}{V_{dc}}, \qquad D_{q2} = \frac{V_q + \omega L_2 I_{d2}}{V_{dc}},$$

$$I_{d1} = \frac{V_d}{R} - \omega C V_q, \qquad I_{d2} = \frac{V_d}{R} - \omega C V_q,$$

$$I_{q1} = \frac{V_q}{R} + \omega C V_d, \qquad I_{q2} = \frac{V_q}{R} + \omega C V_d,$$

$$I_z = 0, \qquad \Delta D_z = 0, \tag{2.51}$$

where: R, L_1, L_2, C and V_{dc} are given, V_d and V_q are so controlled that the transformed output phase voltages are as in (2.14). I_{d1}, I_{d2}, I_{q1}, I_{q2}, D_{d1}, D_{d2}, D_{q1}, D_{q2} and ΔD_z are calculated based on the given values and the control objectives.

Assuming that the input DC voltage source is ideal, then

$$\tilde{v}_{dc} = 0 . \tag{2.52}$$

The small-signal model of the single voltage source inverter is

$$\frac{d}{dt}\begin{bmatrix}\tilde{v}_d\\ \tilde{v}_q\\ \tilde{i}_d\\ \tilde{i}_q\end{bmatrix} = \begin{bmatrix} -\frac{1}{RC} & \omega & \frac{1}{C} & 0\\ -\omega & -\frac{1}{RC} & 0 & \frac{1}{C}\\ -\frac{1}{L} & 0 & 0 & \omega\\ 0 & -\frac{1}{L} & -\omega & 0\end{bmatrix}\cdot\begin{bmatrix}\tilde{v}_d\\ \tilde{v}_q\\ \tilde{i}_d\\ \tilde{i}_q\end{bmatrix} + \begin{bmatrix} 0 & 0\\ 0 & 0\\ \frac{V_{dc}}{L} & 0\\ 0 & \frac{V_{dc}}{L}\end{bmatrix}\cdot\begin{bmatrix}\tilde{d}_d\\ \tilde{d}_q\end{bmatrix}. \tag{2.53}$$

The small-signal model of the parallel voltage source inverters can be derived as follows:

$$\frac{d}{dt}\begin{bmatrix}\tilde{v}_d\\ \tilde{v}_q\\ \tilde{i}_{d1}\\ \tilde{i}_{q1}\\ \tilde{i}_{d2}\\ \tilde{i}_{q2}\\ \tilde{i}_z\end{bmatrix} = \begin{bmatrix} \frac{-1}{RC} & \omega & \frac{1}{2C} & 0 & \frac{1}{2C} & 0 & 0\\ -\omega & \frac{-1}{RC} & 0 & \frac{1}{2C} & 0 & \frac{1}{2C} & 0\\ \frac{-1}{L_1} & 0 & 0 & \omega & 0 & 0 & 0\\ 0 & \frac{-1}{L_1} & -\omega & 0 & 0 & 0 & 0\\ \frac{-1}{L_2} & 0 & 0 & 0 & 0 & \omega & 0\\ 0 & \frac{-1}{L_2} & 0 & 0 & -\omega & 0 & 0\\ 0 & 0 & 0 & 0 & 0 & 0 & 0\end{bmatrix}\cdot\begin{bmatrix}\tilde{v}_d\\ \tilde{v}_q\\ \tilde{i}_{d1}\\ \tilde{i}_{q1}\\ \tilde{i}_{d2}\\ \tilde{i}_{q2}\\ \tilde{i}_z\end{bmatrix} + \begin{bmatrix} 0 & 0 & 0 & 0 & 0\\ 0 & 0 & 0 & 0 & 0\\ \frac{V_{dc}}{L_1} & 0 & 0 & 0 & 0\\ 0 & \frac{V_{dc}}{L_1} & 0 & 0 & 0\\ 0 & 0 & \frac{V_{dc}}{L_2} & 0 & 0\\ 0 & 0 & 0 & \frac{V_{dc}}{L_2} & 0\\ 0 & 0 & 0 & 0 & \frac{V_{dc}}{L_1+L_2}\end{bmatrix}\cdot\begin{bmatrix}\tilde{d}_{d1}\\ \tilde{d}_{q1}\\ \tilde{d}_{d2}\\ \tilde{d}_{q2}\\ \Delta\tilde{d}_z\end{bmatrix} \tag{2.54}$$

Figure 2.20 shows the equivalent circuit of the small-signal model. Some terms are omitted because $I_z = 0$ and $\Delta D_z = 0$ provided that the zero-sequence current is controlled to be zero. The z channel is totally independent from the d and q channels.

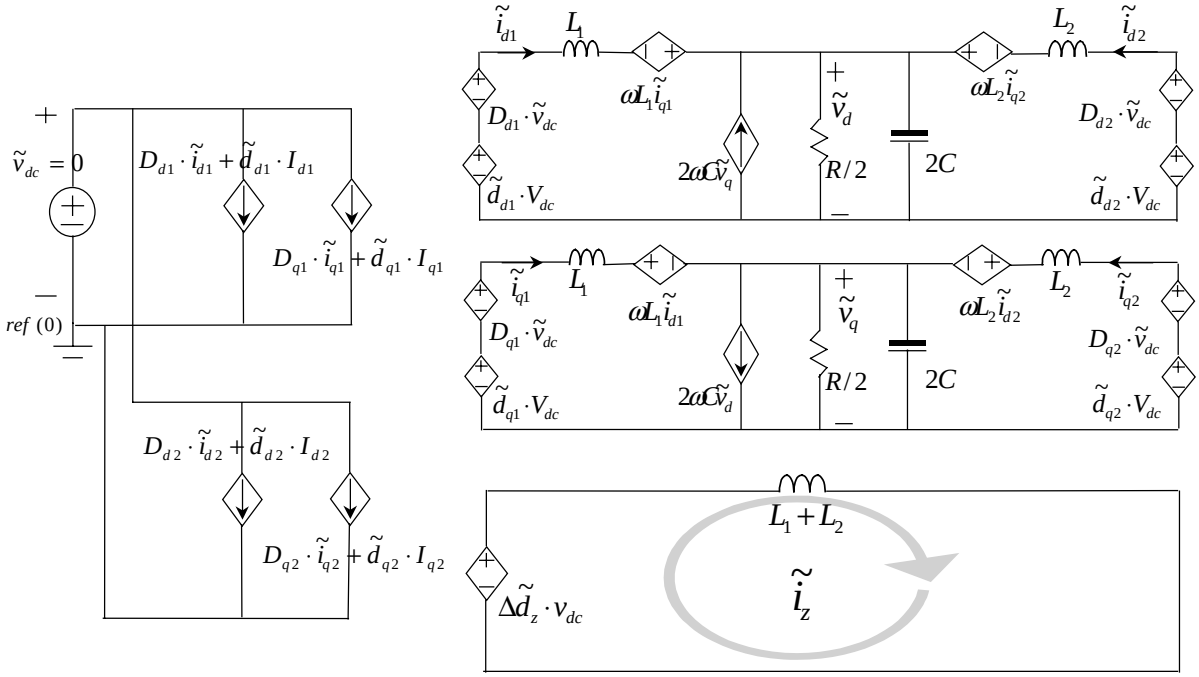

Figure 2.20 Parallel voltage-source inverters' small-signal model.

2.4 INTERACTIONS IN PARALLEL CURRENT-BIDIRECTIONAL CONVERTERS

Because of the direct paralleling, the two converters may have interactions that normally do not appear in the single converter's operation. From the developed models, the following interactions are identified.

2.4.1 Zero-Sequence Interaction

It is obvious from the model that one unique feature of the parallel converters is a zero-sequence interaction, as described in the z channel in Figures 2.14 and 2.18. A further discussion about the zero-sequence interaction and its control is presented in Chapter 4.

2.4.2 Reactive Power Circulation

In a single converter, reactive power could circulate between the source and load if the q channel is not controlled tightly. To the three-phase input voltage source, the three-

phase converter is a load. In the parallel converter system, even if the overall load has a unity power factor to the source, reactive power could still circulate between the two converters. Therefore, it is necessary that each individual converter's current be controlled in phase with its input voltage. This means that the q channel current of each converter must be controlled tightly to zero.

2.4.3 Small-Signal Interaction

To design a compensator, one has to examine the open-loop control-to-output transfer function. Normally, the compensator is designed based on the transfer function when the converter is in single operation. When the converter operates in parallel with others, the transfer function may change due to parallel interactions. To ensure that the compensator will still be valid, the open-loop transfer function needs to be reexamined under the parallel operation condition.

Transfer Functions of Single and Parallel Boost Rectifiers

The plots of the following transfer functions were obtained using MATLAB based on the parameters given below:

$V_m = 120 \cdot \sqrt{2}\ \text{V}$; $\omega = 2\pi \cdot 60\ \text{rad/s}$; $V_{dc} = 400\,\text{V}$; $P_o = 15\text{kW}$; $R = V_{dc}^2 / P_o$; $L = 250\mu\text{H}$; $C = 1200\mu\text{F}$. Be noted that the parallel converter system has 2C and R/2.

Figures 2.21 and 2.22 show transfer functions of the open-loop controls to output currents in both single and parallel operations. The transfer functions with parallel operation have pronounced additional dynamics around line frequency (60Hz, in this case). Figures 2.23 and 2.24 show that the z-channel is decoupled from d and q channels. Figure 2.25 shows that the z channel is a first-order system. It is an integrator because the z channel only has inductance. In practical condition, however, the transfer function has always a certain DC gain due to equivalent series resistance (ESRs) of the inductors and cable resistance. Figure 2.26 shows that the two converters are cross-coupled.

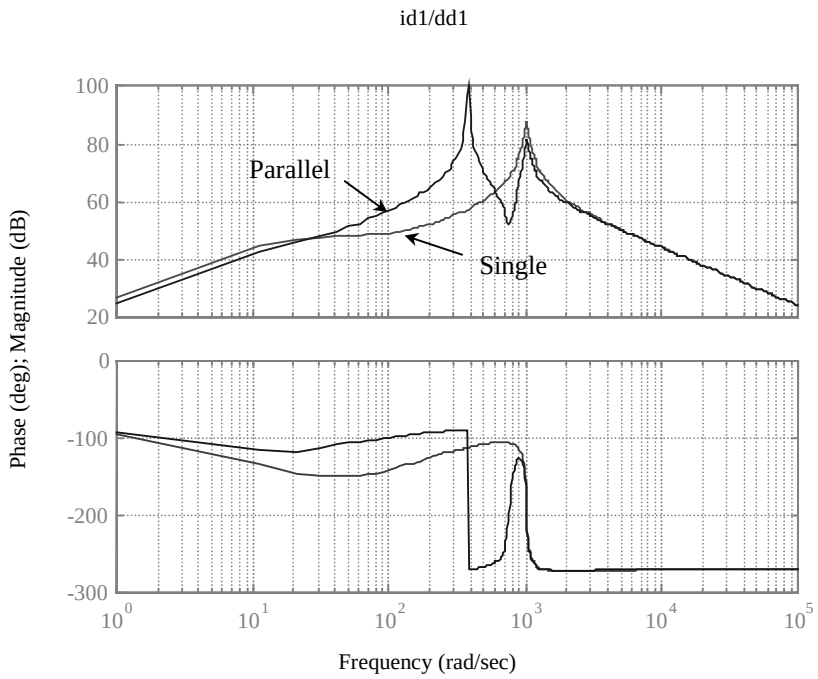

(a) $\tilde{i}_d / \tilde{d}_d$ (single) and $\tilde{i}_{d1} / \tilde{d}_{d1}$ (parallel).

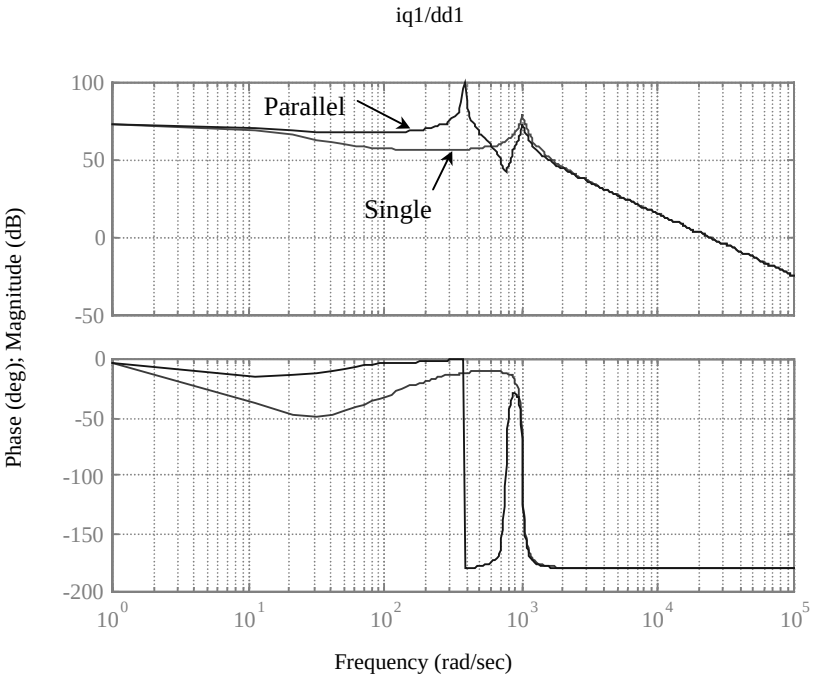

(b) $\tilde{i}_q / \tilde{d}_d$ (single) and $\tilde{i}_{q1} / \tilde{d}_{d1}$ (parallel).

Figure 2.21 Open-loop transfer functions of d-channel control to d- and q-channel currents.

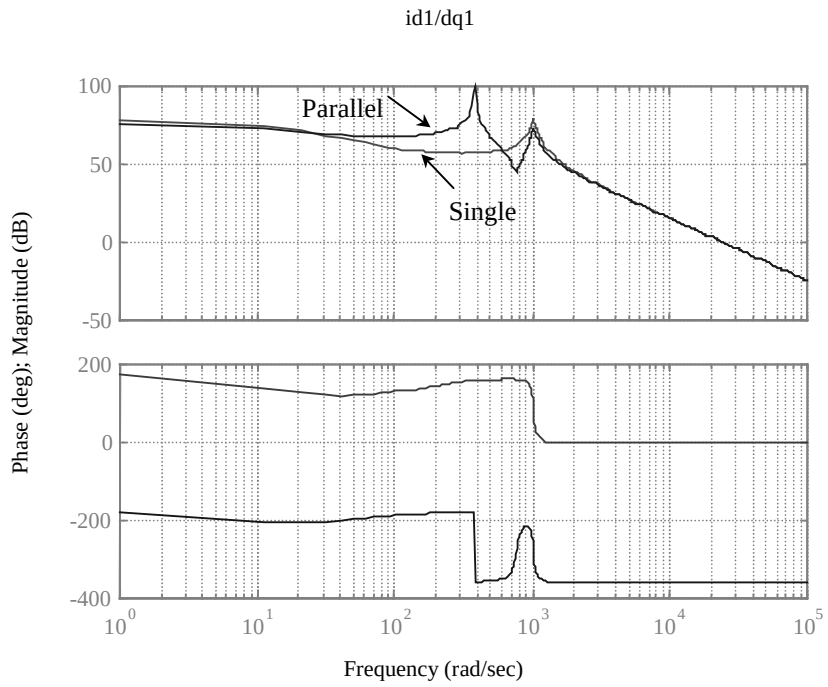

(a) $\tilde{i}_d / \tilde{d}_q$ (single) and $\tilde{i}_{d1} / \tilde{d}_{q1}$ (parallel).

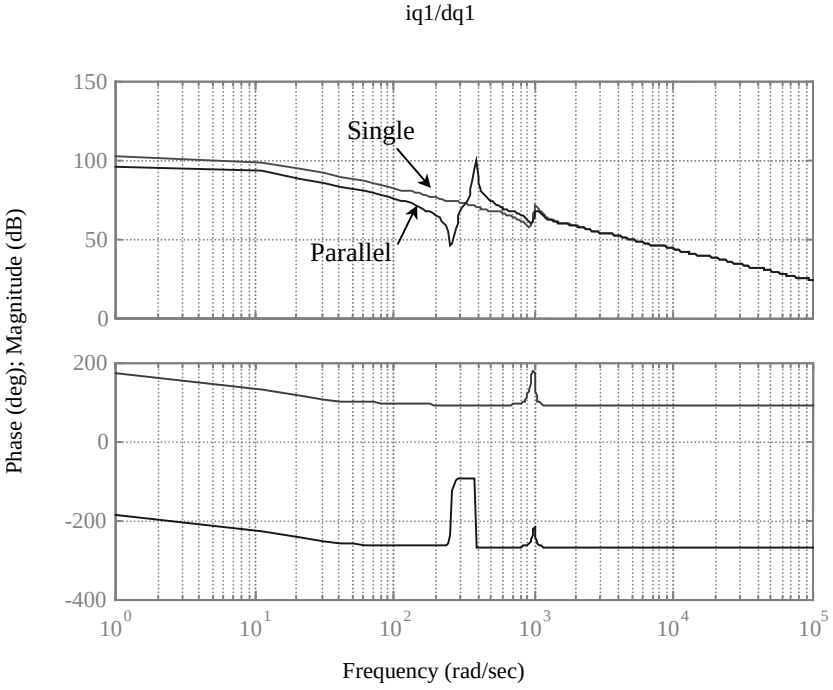

(b) $\tilde{i}_q / \tilde{d}_q$ (single) and $\tilde{i}_{q1} / \tilde{d}_{q1}$ (parallel).

Figure 2.22 Open-loop transfer functions of q-channel control to d- and q-channel currents.

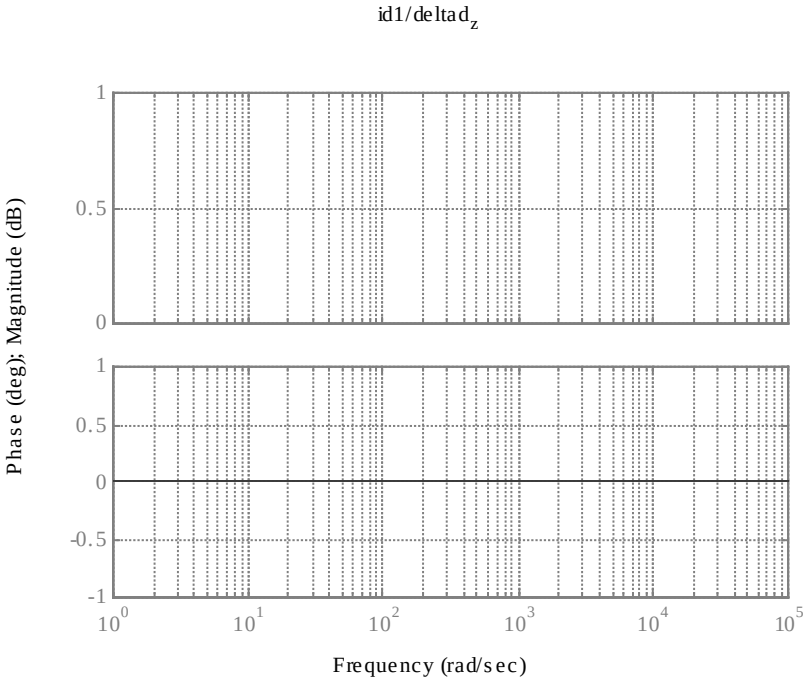

(a) $\tilde{i}_{d1} / \Delta\tilde{d}_z$.

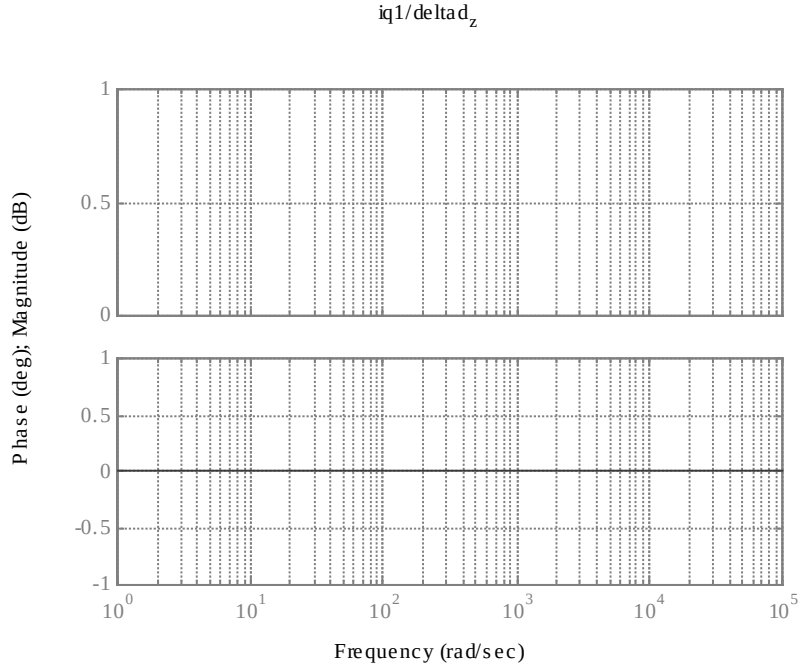

(b) $\tilde{i}_{q1} / \Delta\tilde{d}_z$.

Figure 2.23 Open-loop transfer functions of z-channel control to d- and q- channel currents.

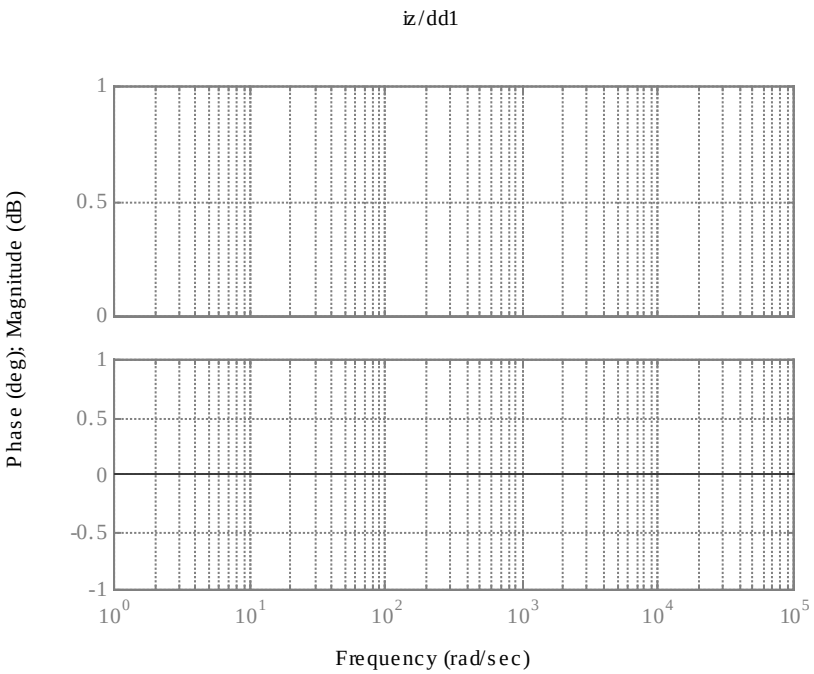

(a) $\tilde{i}_z / \tilde{d}_{d1}$.

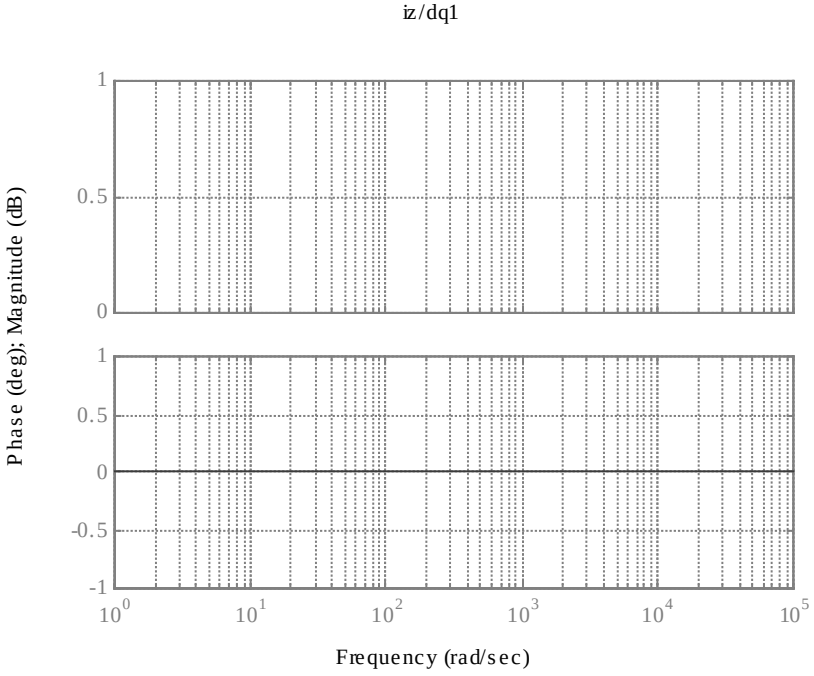

(b) $\tilde{i}_z / \tilde{d}_{q1}$

Figure 2.24 Open-loop transfer functions of d- and q-channel controls to z-channel current.

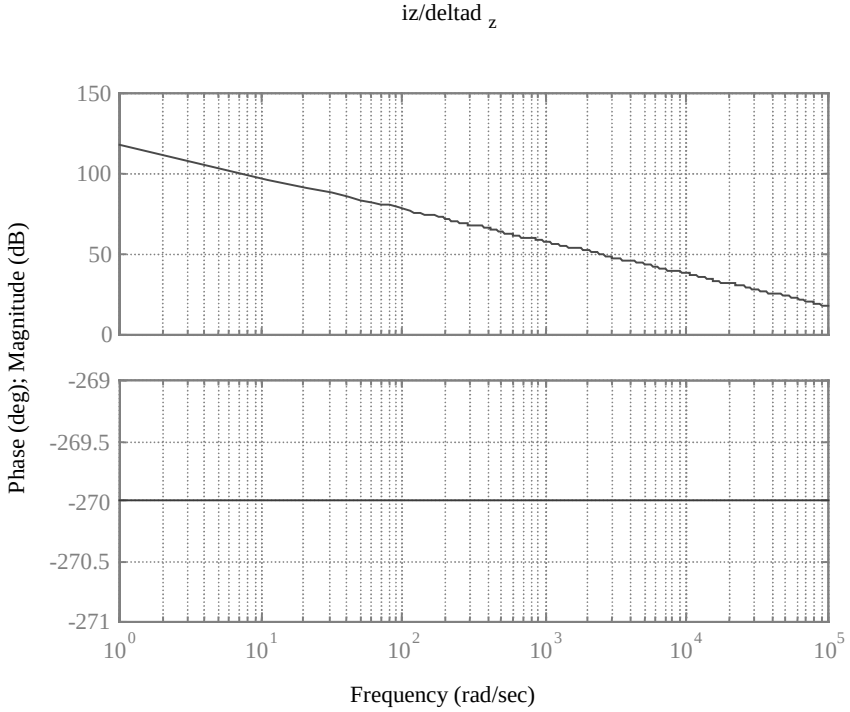

Figure 2.25 Open-loop transfer function of z-channel control to z-channel current $\tilde{i}_z / \Delta\tilde{d}_z$.

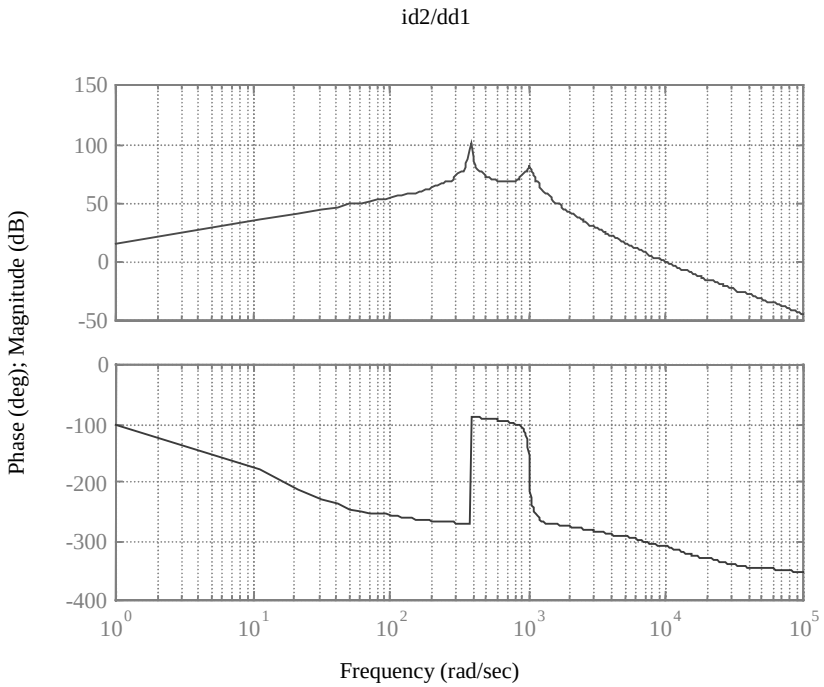

(a) $\tilde{i}_{d2} / \Delta\tilde{d}_{d1}$.

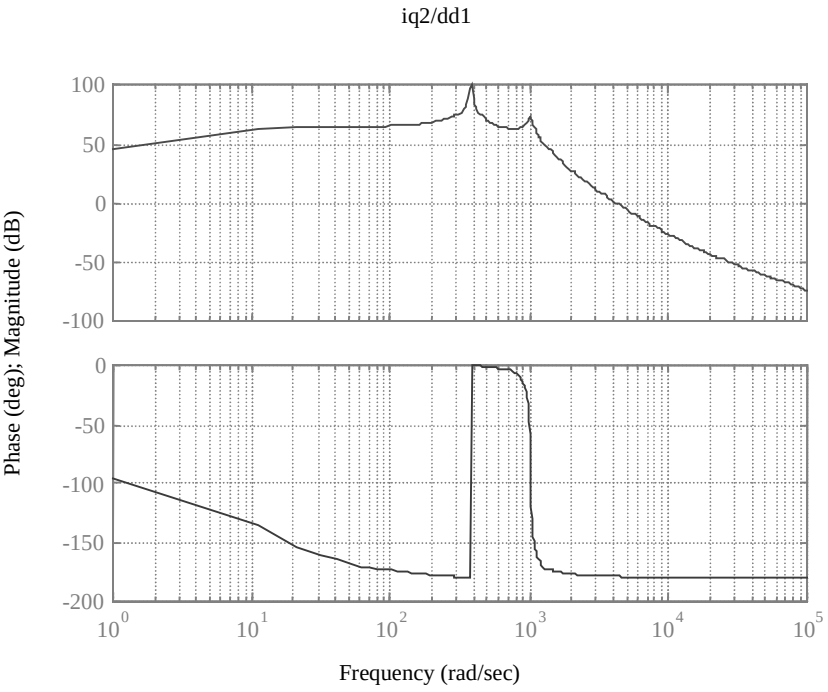

(b) $\tilde{i}_{q2} / \tilde{d}_{d1}$

Figure 2.26 Open-loop transfer functions showing the two converters are cross-coupled.

A prominent difference between single and parallel operation is in the control-to-inductor current transfer functions. The parallel transfer functions have an additional double pole and a double zero.

Since the parallel converters constitute a high-order dynamic system, the complete analytical derivation of these transfer functions is cumbersome. However, general forms and plots of the transfer functions can be obtained using mathematical software, such as MATLAB. For example, the symbolic expressions for the transfer functions $\tilde{i}_d/\tilde{d}_d$ and $\tilde{i}_{d1}/\tilde{d}_{d1}$ have general forms:

$$\tilde{i}_d / \tilde{d}_d = \frac{\mathrm{K} \cdot (\mathrm{s/z} + 1)}{(\mathrm{s/p} + 1)(\mathrm{s/p}^* + 1)}, \tag{2.55}$$

$$\tilde{i}_{d1} / \tilde{d}_{d1} = \frac{\mathrm{K}_1 \cdot (\mathrm{s/z}_1 + 1)}{(\mathrm{s/p}_1 + 1)(\mathrm{s/p}_1^* + 1)} \cdot \frac{(s/z_p + 1)(s/z_p^* + 1)}{(s/p_p + 1)(s/p_p^* + 1)}, \tag{2.56}$$

where * denotes a complex conjugate. The transfer function $\tilde{i}_{d1}/\tilde{d}_{d1}$ has additional terms marked in italics. The italicized terms reflect the interactions between the two converters.

The additional terms are introduced by the parallel interactions. They have the following three features. First, one coupling term is a complex double pole, p_p and p_p^*. The resonant frequency of the double pole is exactly the same as the rotating frequency in the transformation (2.15). Whatever the values of the other parameters, such as input inductance and DC capacitance, this double-pole resonant frequency is always the same as the rotating frequency. Second, the other coupling term is a double zero, z_p and z_p^*. The double zero has a resonant frequency that is close to the resonant frequency of the double pole, p_p and p_p^*, in almost all operating conditions (high line, low line, heavy load or light load). Third, the resonant frequencies of both the double pole and the double zero are lower than the system double pole, p_1 and p_1^*, for all practical designs.

The physics behind the double pole can be explained as follows. Mathematically, a signal with the rotating frequency in the rotating coordinates corresponds to a signal with zero frequency, or DC, in the stationary coordinates due to the rotating transformation in (2.15). Since the double pole is exactly at the rotating frequency in the rotating coordinates, a pole at the DC origin in the stationary coordinates can be found. After examining the model in the stationary coordinates in Figure 2.12, it is found that, if the

control duty cycle in one phase has a DC perturbation, the phase inductor current will become infinite because of the zero-sequence current path. Therefore, it is concluded that the new small-signal interactions in the parallel converters are essentially due to the zero-sequence interaction.

To design the current loop, a proportional-integral controller is used in order to guarantee the unity input current displacement factor. The current loop gains of both the single converter and the two parallel converters are shown in Figure 2.27. The plots were obtained using Saber. It can be seen that the two loop gains practically have the same crossover frequency and the same phase margin. This is due to the fact that the coupling double pole and double zero are around the rotating frequency, which is much lower than the loop-gain crossover frequency. Prior to the cross over frequency, the closed-loop response is dominated by the compensator characteristics.

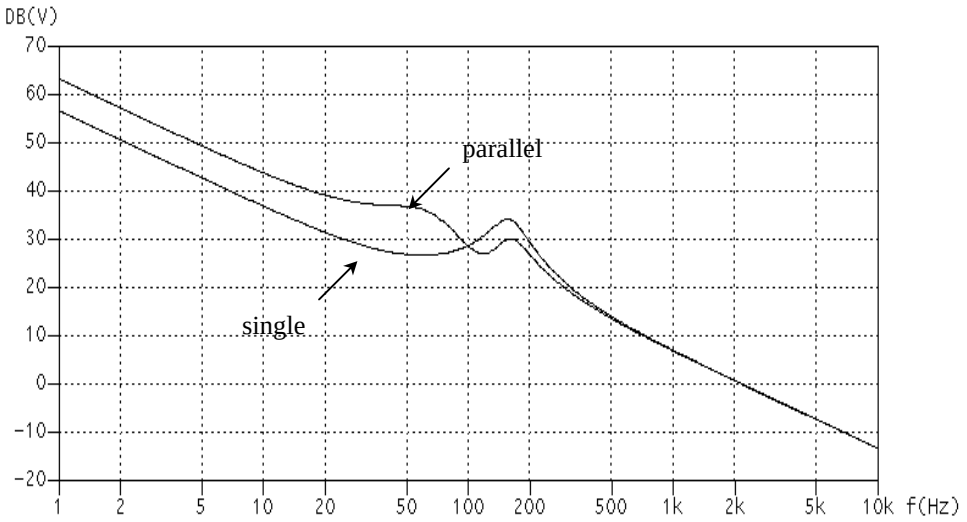

(a) Gain

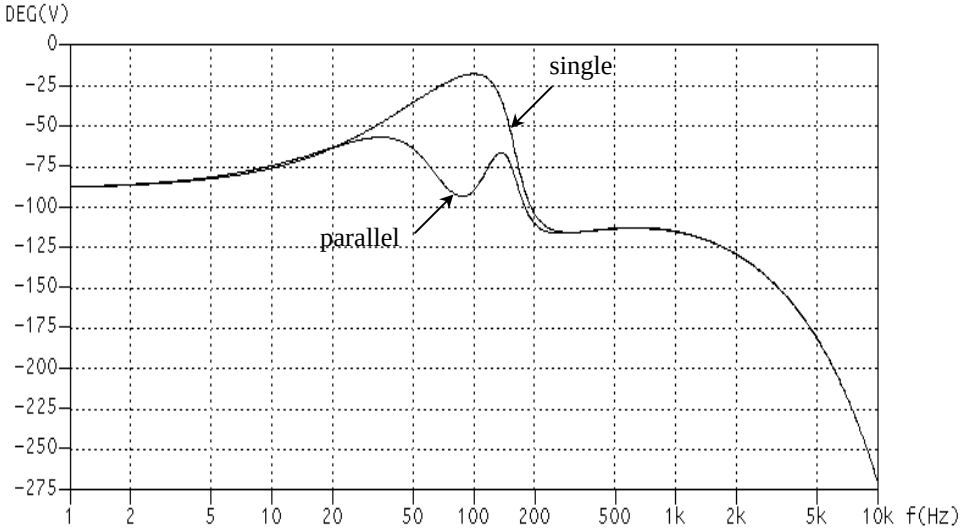

(a) Phase

Figure 2.27 D-channel current-loop gains of single and parallel boost rectifiers.

These transfer functions show that, although the parallel converters are coupled, the coupling double pole and double zero practically cancel each other. Thus, the basic characteristics of the parallel converters' open-loop controls to currents transfer functions are very similar to those of the single converter. This conclusion is very important in that the well-established current loop control design procedure for a single three-phase converter can still be used for individual converter design even if they are in parallel operation. Besides, with a zero-sequence current control loop closed, (as will be

discussed in Chapter 4), the small-signal interaction of the double pole and double zero can be practically eliminated.

Transfer Functions of Single and Parallel Voltage Source Inverters

Similar to parallel three-phase boost rectifiers, Figure 2.28 shows that the z-channel is a first-order system. Figures 2.29 and 2.30 show that the parallel operation introduces additional dynamics around the rotating frequency. Figures 2.31 and 2.32 show that the z channel is decoupled from d and q channels. Figure 2.33 shows that the two converters are cross-coupled.

The plots were obtained using MATLAB based on the parameters below:

$V_m = 120 \cdot \sqrt{2}$ V; $\omega = 2\pi \cdot 60$ rad/s; $V_{dc} = 400$ V; $P_o = 15$kW; $R = V_{dc}^2 / P_o$; $L = 250\mu$H; $C = 1200\mu$F. Be noted that the parallel converter operation has 2C and R/2.

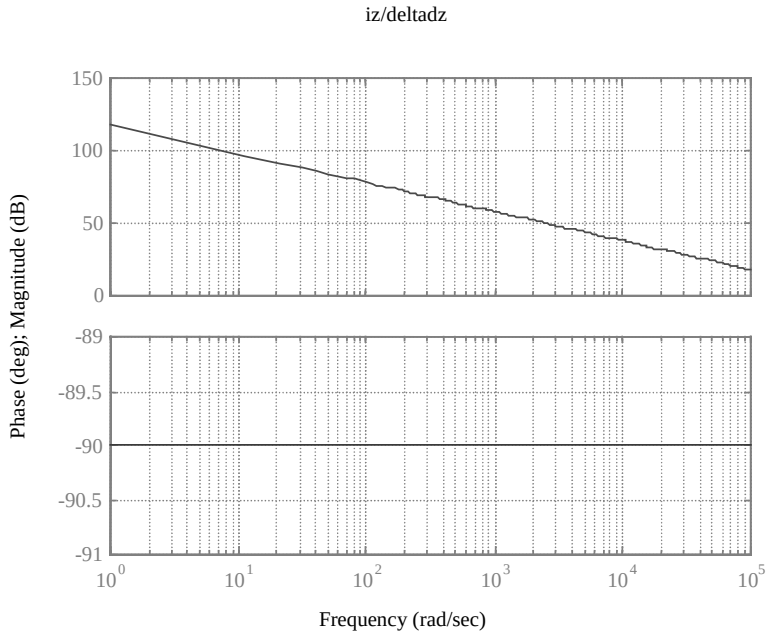

Figure 2.28 Open-loop transfer function of z-channel control to current $\tilde{i}_z / \Delta\tilde{d}_z$.

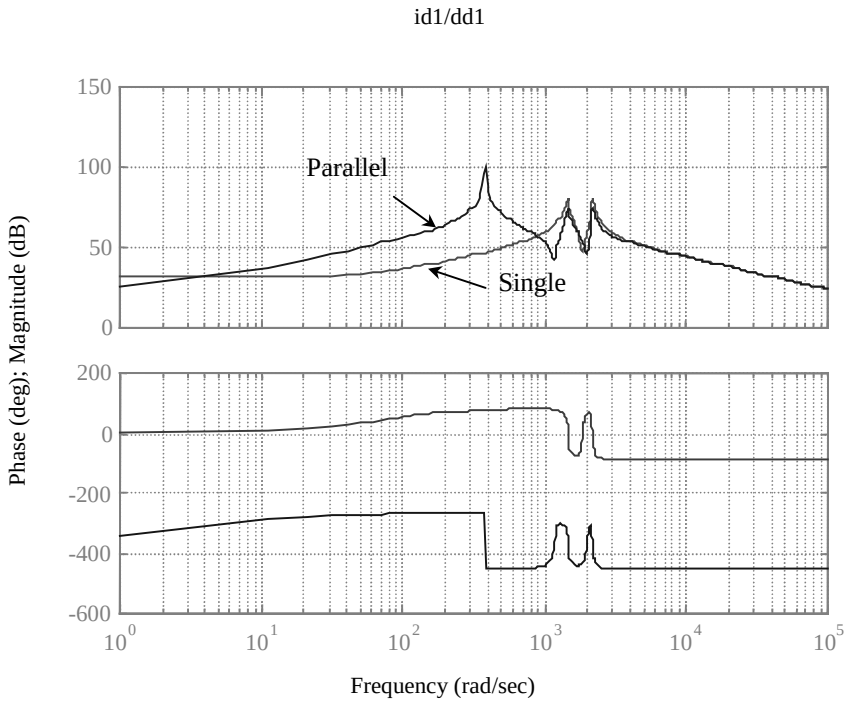

(a) $\tilde{i}_d / \tilde{d}_d$ (single) and $\tilde{i}_{d1} / \tilde{d}_{d1}$ (parallel).

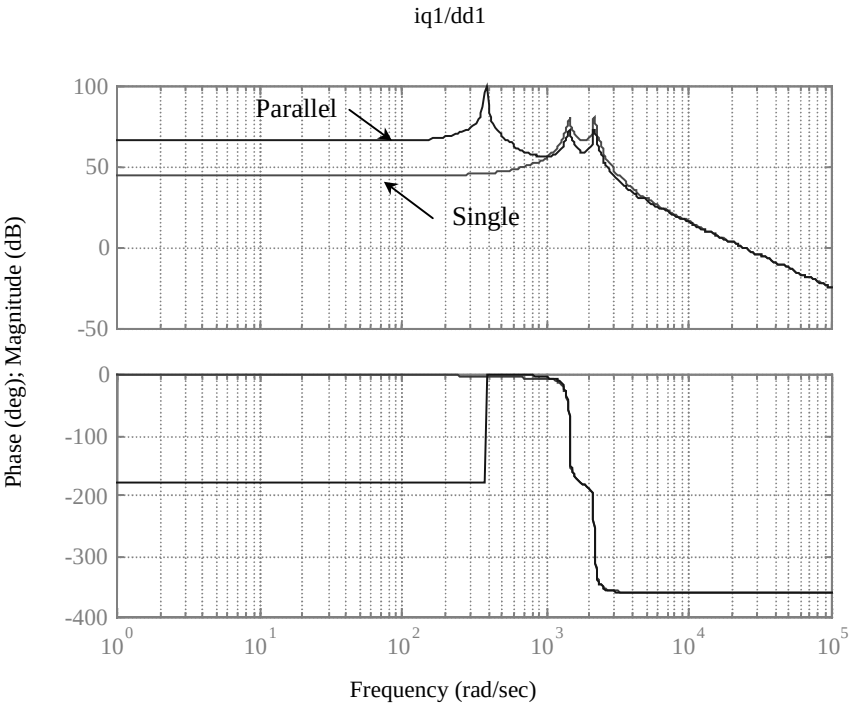

(b) $\tilde{i}_q / \tilde{d}_d$ (single) and $\tilde{i}_{q1} / \tilde{d}_{d1}$ (parallel).

Figure 2.29 Open-loop transfer functions of d-channel control to d- and q-channel currents.

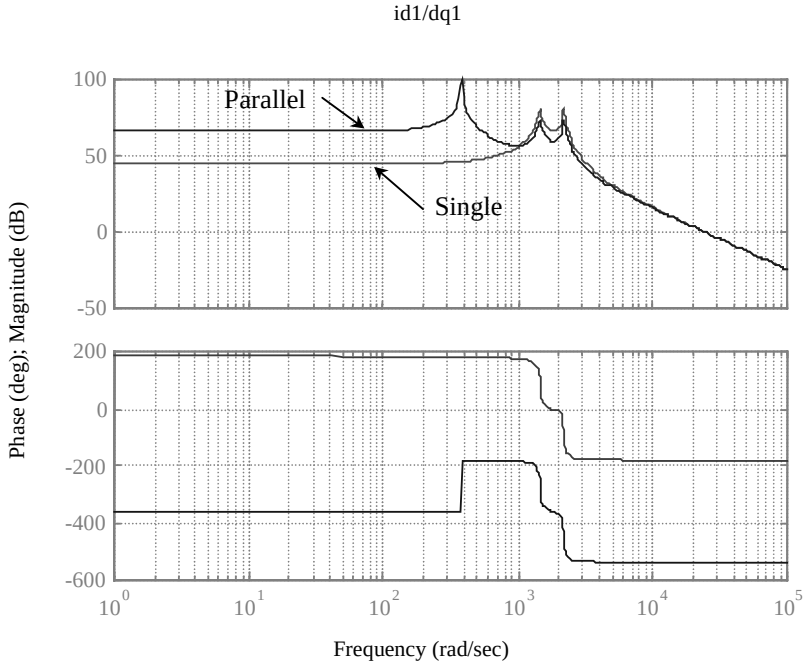

(b) $\tilde{i}_q / \tilde{d}_q$ (single) and $\tilde{i}_{q1} / \tilde{d}_{q1}$ (parallel).

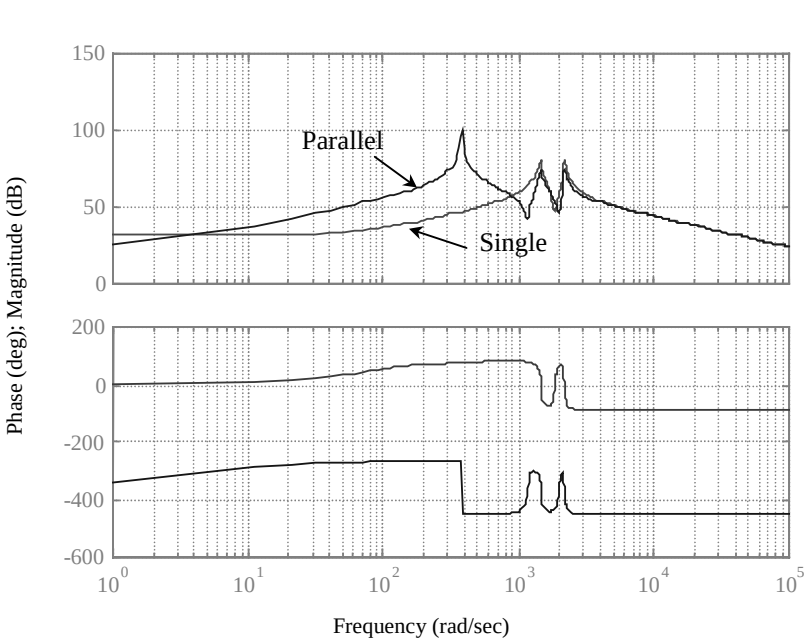

(b) $\tilde{i}_q / \tilde{d}_q$ (single) and $\tilde{i}_{q1} / \tilde{d}_{q1}$ (parallel).

Figure 2.30 Open-loop transfer functions of q-channel control to d- and q-channel currents.

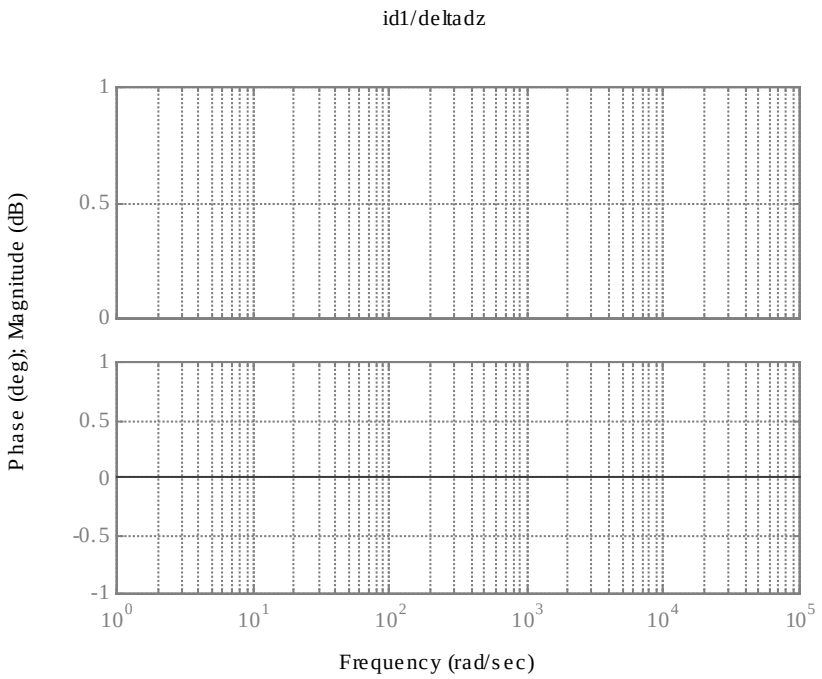

(a) $\tilde{i}_{d1} / \Delta\tilde{d}_z$.

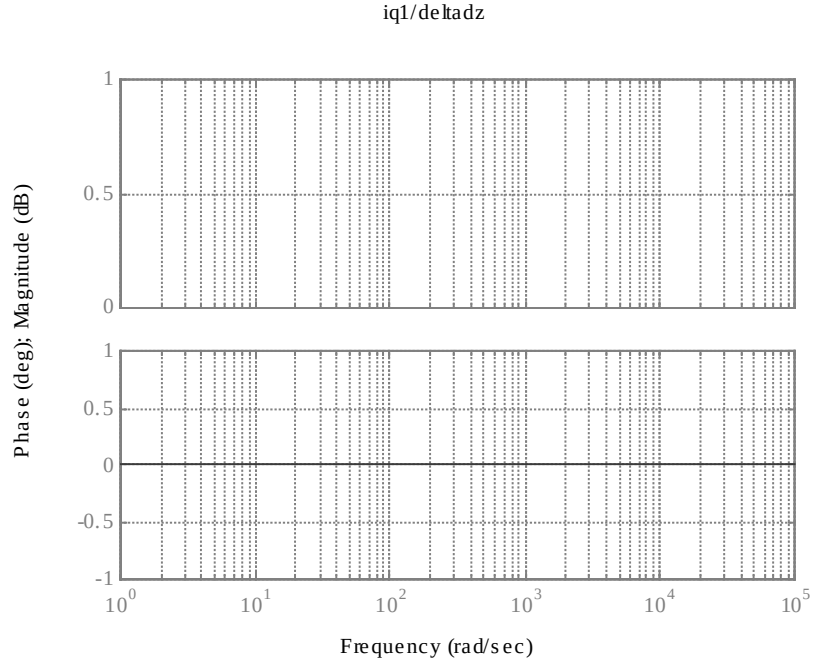

(b) $\tilde{i}_{q1} / \Delta\tilde{d}_z$.

Figure 2.31 Open-loop transfer functions of z-channel control to d- and q-channel currents.

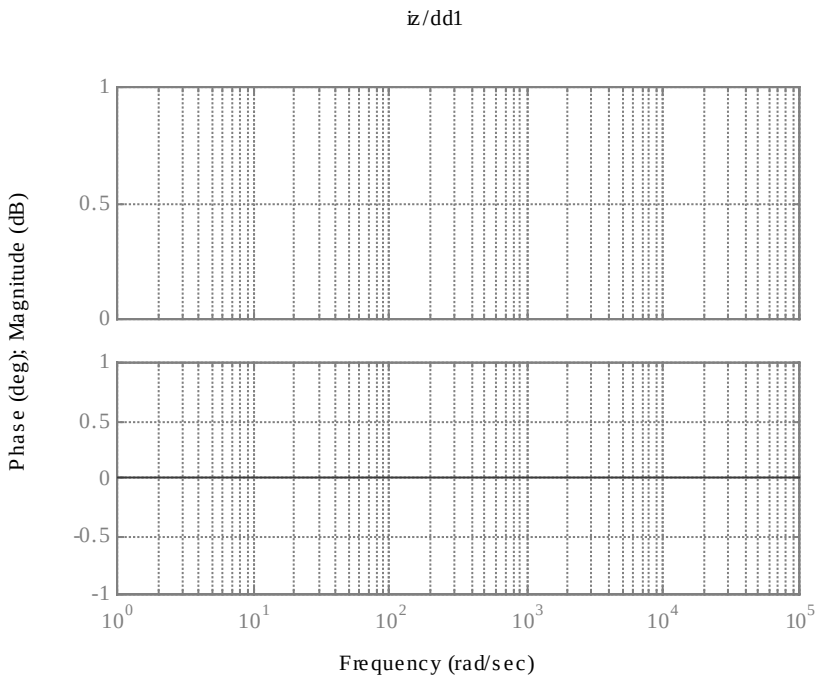

(a) $\tilde{i}_z / \tilde{d}_{d1}$.

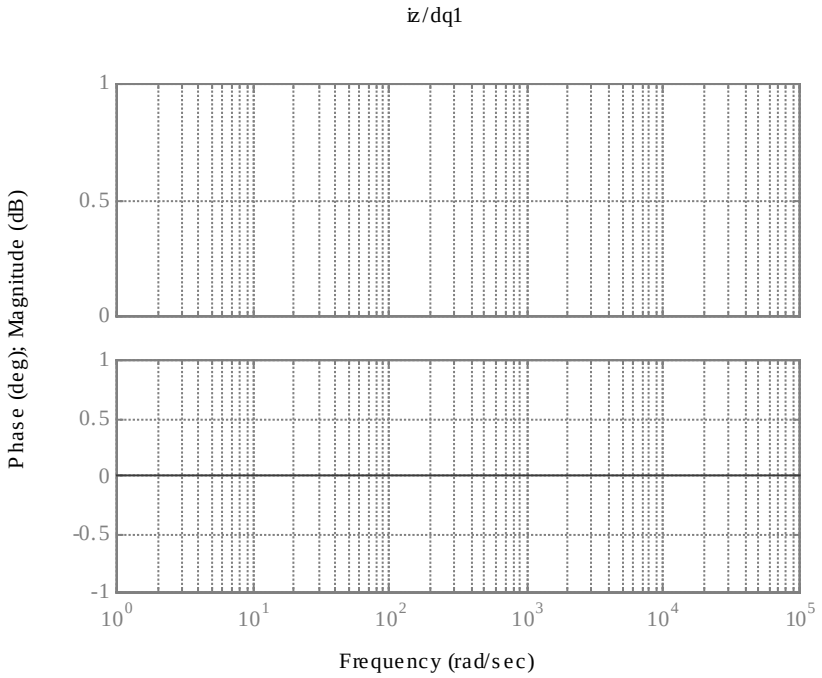

(b) $\tilde{i}_z / \tilde{d}_{q1}$.

Figure 2.32 Open-loop transfer functions of d- and q-channel controls to z-channel current.

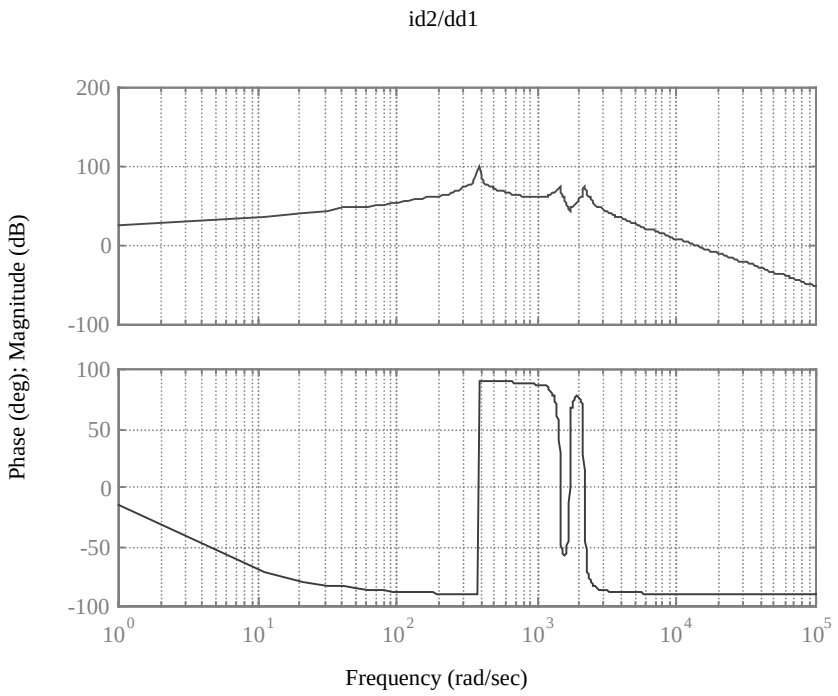

(a) $\tilde{i}_{d2} / \tilde{d}_{d1}$

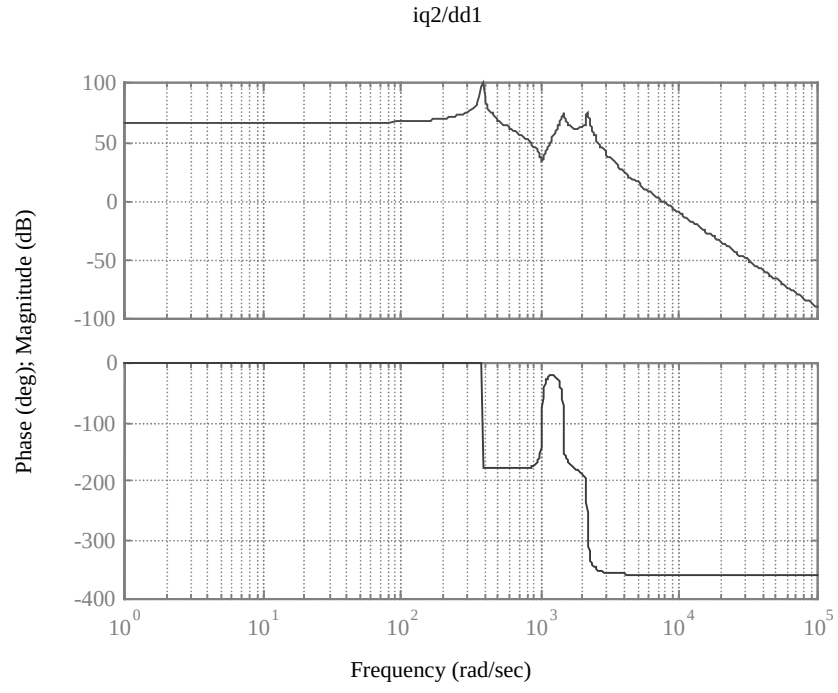

(b) $\tilde{i}_{q2} / \tilde{d}_{d1}$

Figure 2.33 Open-loop transfer functions showing the two converters are cross-coupled.